Structure-Photochemical Function Relationships in Nitrogen-Containing Heterocyclic Aromatic Photobases Derived from Quinoline

Sophya F. Alamudun, Kyle Tanovitz, April Fajardo, Kaitlind Johnson, Andy Pham,

Tina Jamshidi Araghi, and Andrew S. Petit*

Department of Chemistry and Biochemistry, California State University, Fullerton, California

92834-6866, United States

*Author to whom correspondence should be addressed. Email: apetit@fullerton.edu

Abstract

Photobases are compounds which become strong bases after electronic excitation. Recent experimental studies have highlighted the photobasicity of the 5-R quinoline compounds, demonstrating a strong substituent dependence to the pK_a^*. In this paper we describe our systematic study of how the photobasicity of four families of nitrogen-containing heterocyclic aromatics are tuned through substituents. We show that substituent position and identity both significantly impact the pK_a^*. We demonstrate that the substituent effects are additive and identify many disubstituted compounds with substantially greater photobasicity than the most photobasic 5-R quinoline compound identified previously. We show that the addition of a second fused benzene ring to quinoline, along with two electron-donating substituents, lowers the $S_0 \rightarrow S_{CT}$ vertical excitation energy into the visible while still maintaining a $pK_a^* > 14$. Overall, the structure-function relationships developed in this study provide new insights to guide the development of new photocatalysts that employ photobasicity.

Introduction

Photocatalysts are of widespread interest to the chemistry community because of their important role in the transformation of solar light into chemical energy as well as the ability to systematically control catalyst reactivity using light. In processes like artificial photosynthesis, photocatalysts make possible redox reactions which require the overall transfer of multiple electrons and protons. This chemistry is driven by the rearrangement of charge in the photocatalyst after excitation to a state with significant charge-transfer character. This redistribution of charge in the electronic excited state allows electron or proton transfer reactions to occur which would otherwise be thermodynamically and/or kinetically unfavorable in the ground state.

Excited-state proton transfer represents a specific manifestation of photocatalysis that has also been applied to the optical control of enzymes as well as a probe of local molecular environments.[1–3] Previous experimental and theoretical investigations of systems which exhibit excited-state proton transfer have primarily focused on photoacids, molecules which become stronger proton donors after electronic excitation ($pK_a^* < pK_a$).[4–11] The gains in acid strength with photoexcitation can be very large, with examples reported in the literature of molecules whose K_a^* is 12 orders of magnitude larger than its K_a.[9] Interestingly, photobases, molecules which become stronger proton acceptors after electronic excitation, are much less well represented in the literature despite their potential application in photocatalysis.[12–19]

Recent experimental studies performed in the Dawlaty lab have investigated the photochemical properties of a family of 5-R quinoline derivatives.[20–25] These compounds were all shown to be photobases, with the magnitude of the photobasicity depending strongly on the identity of the substituent. Specifically, photoexcitation results in K_b increasing by over 10 orders of magnitude when the substituent is the electron-donating NH_2 group but only approximately 2

orders of magnitude when the substituent is the electron-withdrawing CN group. This behavior

has been attributed to the charge-transfer character of the singlet bright state responsible for the

photobasicity, S_{CT}. Specifically, the $S_0 \rightarrow S_{CT}$ transition results in an increase of electron density

on the ring nitrogen atom and hence an increase in its basicity. Electron-donating substituents

amplify the charge-transfer character of the transition, leading to larger pK_a^*.

As a further step towards practical photocatalysts employing photobasicity, a recent study

reported two iridium complexes containing a pendant quinoline ligand.[23] This study demonstrated

that the quinoline moiety maintained its photobasicity in the complexes and as such, represents the

first rational design of a transition metal complex in which a ligand exhibits light-triggered proton

removal functionality.

While these studies demonstrate the potential of applying photobasicity in photocatalyst

design, only a very limited family of photobases has been systematically studied to date. In this

paper, we report a computational investigation of structure-function relationships in the

photobasicity of nitrogen-containing heterocyclic aromatics related to quinoline. We

demonstrate that both substituent identity and position matter in determining the thermodynamic

driving force for excited state protonation. We show that the substituent effects are additive,

with a number of quinoline and isoquinoline derivatives with multiple electron-donating

substituents identified to have K_b^* that are several orders of magnitude larger than that of the

strongest monosubstituted quinoline photobase identified in experiment, 5-aminoquinoline. We

demonstrate that the addition of a second fused benzene ring lowers the $S_0 \rightarrow S_{CT}$ excitation

energy while also decreasing the extent of photobasicity; similar conclusions were recently

drawn by Hunt et al.[24] However, we identify a number of acridine and 1-azaanthracene

derivatives which are both strong bases in the S_{CT} excited state and have $S_0 \rightarrow S_{CT}$ excitation

energies that are in the visible. Collectively, this work further refines the design principles

necessary to develop new photocatalysts which employ photobasicity.

Theoretical Methods

Figure 1 illustrates the Förster cycle used to calculate ΔG^* and hence pK_a^* from a series

of quantities that are readily obtained from electronic structure calculations, specifically $\Delta G^* =$

$\Delta G + \Delta E_{00}^B - \Delta E_{00}^{BH}$. In this equation, the ground state ΔG is related to ΔG^* through the

adiabatic S_{CT}-S_0 energy gaps of the base and conjugate acid, ΔE_{00}^B and ΔE_{00}^{BH}. More specifically,

$\Delta E_{00}^B = E_{S_{CT}}^B - E_{S_0}^B$, where $E_{S_{CT}}^B$ is the electronic energy of the charge-transfer S_{CT} state at the

S_{CT} minimum energy geometry while $E_{S_0}^B$ is the S_0 electronic energy at the S_0 minimum energy
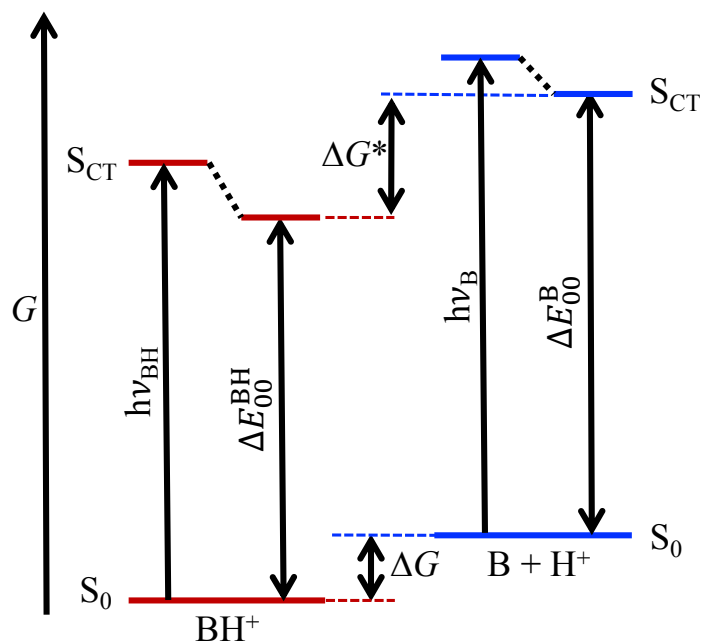
geometry.

Figure 1: The Förster cycle used to calculate ΔG^*
from ΔG and the adiabatic S_{CT}-S_0 energy gap for the
base and conjugate acid (ΔE_{00}^B and ΔE_{00}^{BH}). Vibrational
relaxation on S_{CT} is denoted by the dotted black lines.

The first step is calculating the ground state free energies of B and BH$^+$, G_B and G_{BH},

where the geometry optimizations and vibrational frequency evaluations are performed at the

ωB97XD/def2-svpd level of theory while the electronic energies are subsequently evaluated

using ωB97XD/def2-tzvppd.[26,27] All DFT calculations employ a (99,590) integration grid.

Solvent effects are included using a polarizable continuum model (PCM); a conductor-like PCM

(CPCM) for the geometry optimizations and an integral equation formalism PCM (IEF-PCM) for

the single-point calculations.[28] Both PCM models use a cavity constructed with Bondi radii and

switching Gaussian surface charges.[29,30] As in the experiments, the solvent used in these

calculations is water. All electronic structure calculations were performed using the Q-Chem 5.1

software package.[31]

Figure 2 demonstrates that the calculated G_B-G_{BH} is very strongly correlated with the

experimental pK_a of BH$^+$ for the family of 5-R-quinoline derivatives considered by Dawlaty and

coworkers.[20] Indeed, we take Figure 2 to provide a suitable calibration curve to convert G_B-G_{BH}

into pK_a for other N-containing aromatic heterocycles where the basicity involves a sp^2

hybridized lone pair on N. The desired ΔG is then easily calculated from the pK_a using $\Delta G = 2.303RTpK_a$. Finally, note that 5-bromoquinoline is excluded from the linear regression

analysis presented in Figure 2 because it did not follow the same trend as the other 5-R quinoline
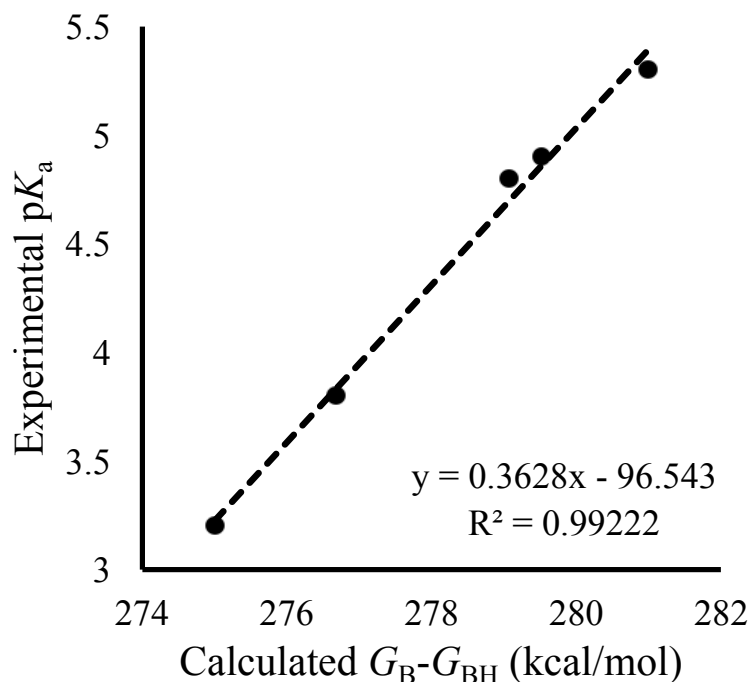
compounds.

Figure 2: Correlation between the experimental pK_a of the 5-R quinoline compounds studied by Dawlaty and coworkers and the calculated difference in free energy between the base and conjugate acid (G_B-G_{BH}).[20] Note that 5-bromoquinoline was not included in the above analysis because it did not follow the trend formed by the other 5-R quinoline compounds.

The remaining quantities, ΔE_{00}^B and ΔE_{00}^{BH}, are the adiabatic S_{CT}-S_0 energy gaps for the base and conjugate acid. The excited state geometry optimizations are performed at the TD-DFT/ωB97XD/def2-svpd level of theory within the Tamm-Dancoff approximation (TDA) while the single-point calculations are performed using TD-DFT/ωB97XD/def2-tzvppd without the TDA. TDA is used in the excited state geometry optimizations to avoid numerical singularities that can arise when full TD-DFT is used to explore potential energy surfaces.[32] All TD-DFT calculations used a (99,590) integration grid. As above, solvent effects are included using PCM, with CPCM used in the excited state geometry optimizations and state-specific IEF-PCM used for the single-point calculations.[33,34] The PCM models were parameterized for water with cavities constructed using Bondi radii and switching Gaussian surface charges.

Our choice of the ωB97XD functional for this study is motivated in part because it is a long-range corrected functional. Long-range corrected functionals are known to reduce the self-interaction error in DFT and provide an improved description of charge-transfer states in TD-DFT calculations.[35] In particular, TD-DFT calculations performed using the ωB97XD functional have been shown to provide a reasonable description of the low-lying singlet states of heteroaromatics, in particular S_{CT}.[36,37]

Throughout this study, we identify S_{CT} as the lowest-energy $\pi \rightarrow \pi^*$ bright state of the bases for which the ring nitrogen gains charge density and hence becomes more basic. Analysis of the electronic character of the excitations is performed using natural transition orbitals and Löwdin charge differences.[38,39] The highest occupied natural transition orbitals (HONTO) and the lowest unoccupied natural transition orbital (LUNTO) associated with S_{CT} are shown in Figure 3 for two representative compounds considered in this study; other examples can be found in the Supporting Information. In particular, Figure 3 shows that S_{CT} is $\pi \rightarrow \pi^*$ with charge-transfer character, with electron density on the amine groups shifting into the rest of the molecule. We further ensure that the chosen state for the acid form of the compounds has the same electronic character as the base. For the majority of the compounds considered in this study, particularly those with strongly electron-donating substituents, S_{CT} is identified as S_1. State-tracking is used during the excited state geometry optimizations to ensure that the electronic character of the excited state is preserved.[40] We additionally verify that the natural transition orbitals of the S_{CT} state are consistent at the S_0 and S_{CT} optimized geometries.

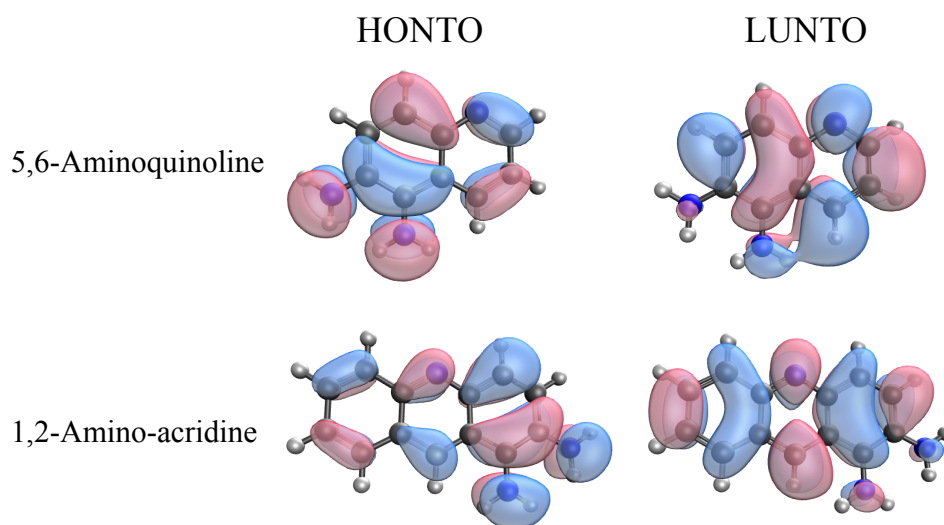|	HONTO	LUNTO

5,6-Aminoquinoline

1,2-Amino-acridine

Figure 3: The highest occupied natural transition orbital (HONTO) and lowest unoccupied transition orbital (LUNTO) associated with the S_{CT} state of 5,6-aminoquinoline and 1,2-amino-acridine. These orbitals were calculated at the S_{CT} optimized geometry and plotted with an isovalue of 0.06.

Results and Discussion

Analysis of the Photobasicity of the Monosubstituted Quinolines

Figure 4 shows that the calculated pK_a^* for the 5-R quinoline compounds depends strongly on the Hammett σ_{para}^+ of the substituent.[41,42] Specifically, electron-withdrawing substituents ($\sigma_{para}^+ > 0$) lower the pK_a^* while electron-donating substituents ($\sigma_{para}^+ < 0$) raise the pK_a^*. The corresponding K_b^* span nearly 10 orders of magnitude, with $K_b^* =2.69\text{x}10^{-8}$ for 5-cyanoquinoline and $K_b^* =205$ for 5-dimethylaminoquinoline. Note that all compounds with $pK_a^* > 14$ are strong bases in the S_{CT} excited electronic state. In contrast with the excited state basicity, the variation in the ground state basicity is much smaller; K_b ranges from $1.67\text{x}10^{-11}$ for 5-cyanoquinoline to $2.48\text{x}10^{-9}$ for 5-aminoquinoline. Finally, Table S1 in the Supporting Information shows that electron-donating substituents decrease the vertical excitation energy of

the 5-R quinoline compounds; the calculated $S_0 \rightarrow S_{CT}$ vertical excitation energy is 4.70 eV for quinoline and 3.69 eV for 5-methylaminoquinoline.
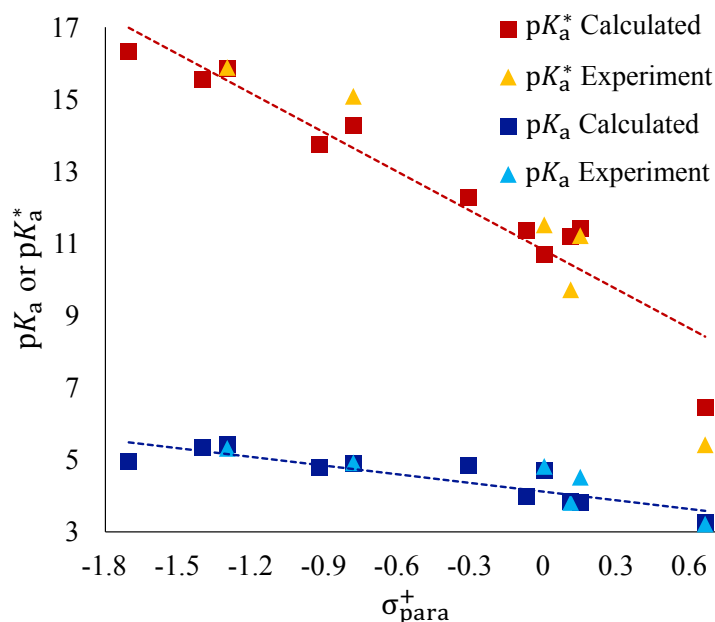

Figure 4: Dependence of our calculated pK_a (blue squares) and pK_a^* (red squares) on the Hammett σ_{para}^+ of the substituent for the 5-R quinoline compounds considered in this study. The Hammett σ_{para}^+ parameterizes the strength of electron-donating ($\sigma_{para}^+ < 0$) or electron-withdrawing ($\sigma_{para}^+ > 0$) character of the substituent. Where available, the corresponding experimental values reported by Dawlaty and coworkers are shown as triangels.[20] The R^2 values for pK_a^* are 0.89 for experiment and 0.91 for theory whereas for pK_a they are 0.76 and 0.75.

Figure 4 additionally compares our calculated pK_a and pK_a^* (squares) to the experimental values reported by Dawlaty and coworkers (triangles).[20] With the exception of 5-bromoquinoline, the agreement between the experimental and calculated pK_a is excellent; 5-bromoquinoline was not included in the analysis shown in Figure 2 because it did not follow the same trend as the other 5-R quinoline compounds. The excellent agreement between the experimental and calculated pK_a reflects our use of the calibration curve developed in Figure 2. While there are some discrepancies between the calculated and experimental pK_a^*, we clearly

capture the same overall trend as experiment. Moreover, the agreement between experiment and theory is best for the strongly photobasic compounds with electron-donating substituents, the class of compounds of interest in this study. The errors that do exist between the calculated and experimental pK_a^* primarily reflect errors in the calculated adiabatic energy gaps that result from our choice of using TD-DFT with a PCM solvent model to describe the electronic excited states. Nevertheless, Figure 4 demonstrates that our chosen computational approach captures the same trend as experiment for how photobasicity is modulated by changes to the molecular structure and hence is suitable for identifying the structure-photochemical function relationships of interest in this study.

Figure 5 extends our analysis of the photobasicity of monosubstituted quinoline to explore the effect of substituent position; the corresponding data is summarized in Tables S2-S6 in the Supporting Information. Compounds with the substituent on the nitrogen-containing ring are shown as squares whereas compounds with the substituent on the fused benzene ring are shown as triangles. The natural transition orbitals involved in the $S_0 \rightarrow S_{CT}$ transition, which are shown for representative compounds in Figures S2 and S3 in the Supporting Information, indicate that the transition is consistently $\pi \rightarrow \pi^*$ regardless of the substituent position.
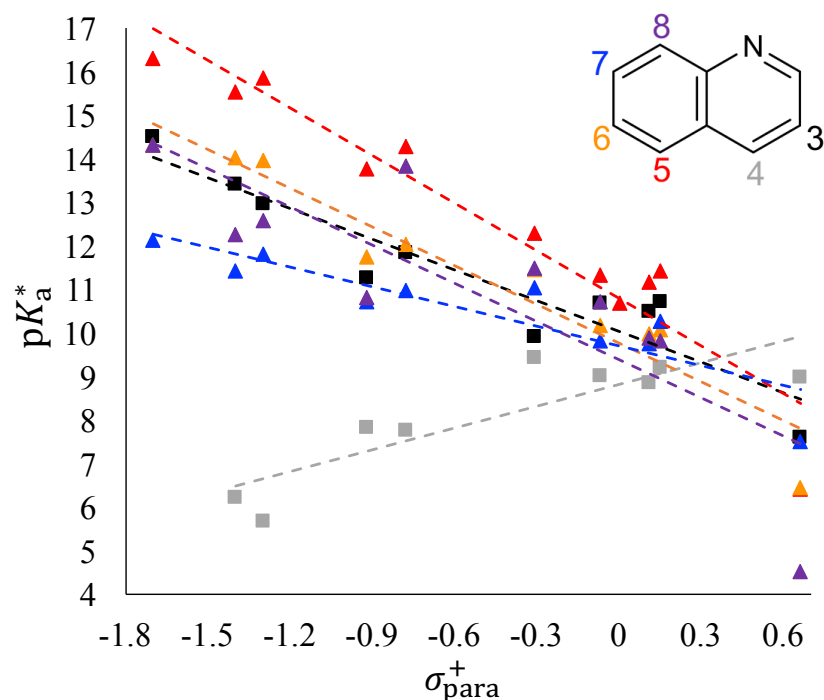
Figure 5: Calculated pK_a^* versus the Hammett σ_{para}^+ parameter of the substituent for the monosubstituted quinoline compounds considered in this study. As shown in Figure S4 in the Supporting Information, R^2 values from the linear regression analysis range from 0.92 for the 6-R quinolines to 0.69 for the 8-R quinolines.

We focus first on the compounds with the substituent on the fused benzene ring. The 5-R quinolines (shown as red triangles) have the largest pK_a^* and hence strongest photobasicity. This is especially apparent for the strongly electron-donating –OH, –NH₂, –NHCH₃, and –N(CH₃)₂ substituents. Turning to the other substituent positions on the fused benzene ring, the 6-R (orange triangles), 7-R (blue triangles), and 8-R (purple triangles) quinolines show the same general trend as the 5-R quinolines, with the pK_a^* increasing as the substituent is made increasingly electron-donating. The 6-R quinoline compounds have significantly larger pK_a^* than the corresponding 7-R quinoline compounds; 6-dimethylaminoquinoline has $pK_a^* = 14.32$ whereas 7-dimethylaminoquinoline has $pK_a^* = 12.13$.

The 8-R quinoline compounds exhibit a greater variability in their pK_a^* than the 5-R, 6-R, and 7-R quinolines. In particular, 8-hydroxyquinoline, 8-aminoquinoline, and 8-methylaminoquinoline have much lower pK_a^* than would be expected based on the trend in the other 8-R quinolines. These three compounds each contain a substituent that is not only a strong electron-donating group but also a hydrogen bond donor. We therefore believe that the anomalously low pK_a^* of these three compounds reflects the presence of intramolecular hydrogen bonding between the ring nitrogen and the neighboring –OH, –NH$_2$, or –NHCH$_3$ substituent. Protonation of the base results in the loss of this intramolecular hydrogen bonding, causing a reduction of the K_b and K_b^* relative to what is expected from the purely electronic effects of the substituent. Further support for this explanation comes from the fact that the *syn* conformer of 8-hydroxyquinoline, which has the hydroxyl group oriented towards the ring nitrogen, is stabilized by 3.25 kcal/mol relative to the *anti* conformer. The observation that 8-methoxyquinoline has a larger pK_a^* than 8-dimethylaminoquinoline additionally suggests that steric repulsion between the protonated ring nitrogen and the neighboring substituent group in the conjugate acids provides an additional reduction in the thermodynamic driving force for excited state protonation; the *anti* conformer of 8-methoxyquinoline avoids this steric repulsion while simultaneously allowing the methoxy group to participate in π conjugation with the rings. Figures S6-S8 in the Supporting Information show representative molecular geometries of 8-R quinoline compounds.

Figure 5 also shows the impact of substituents on the nitrogen-containing ring. The 3-R quinoline compounds (black squares) show a similar trend to the 6-R quinolines with a generally smaller photobasicity. Interestingly, the 4-R quinoline compounds (gray squares) show the opposite trend as the other monosubstituted quinolines, with pK_a^* decreasing as the substituent is

made increasingly electron-donating. Indeed, for 4-aminoquinoline and 4-methylaminoquinoline, electronic excitation results in a decrease in basicity; for example, pK_a=7.28 and pK_a^* =5.69 for 4-aminoquinoline. In contrast to their photobasicity, Tables S1-S6 in the Supporting Information show that 4-aminoquinoline and 4-methylaminoquinoline are the strongest bases in the ground state of all of the monosubsituted quinoline compounds considered in this study. Finally, Figure S5 in the Supporting Information shows that the effect of substituents on the $S_0 \rightarrow S_{CT}$ vertical excitation energy is much smaller for the 4-R quinolines than for the other monosubsituted quinolines.

As mentioned above, photobasicity in the quinoline derivatives has been attributed to the charge-transfer character of the $S_0 \rightarrow S_{CT}$ transition, with the ring nitrogen gaining electron density and hence becoming more basic.[20,24] The extent of charge-transfer character in the $S_0 \rightarrow S_{CT}$ transition can be quantified through the Löwdin charge difference on the ring nitrogen (Δq).[38,39] This analysis can also be performed at the excited-state optimized geometry resulting in Δq^*. Figure 6 shows the dependence of pK_a^* on Δq (squares) and Δq^* (triangles) for the 4-R, 5-R, and 6-R quinolines considered in this study. Figure S9 in the Supporting Information compares pK_a^* and Δq for all of the monosubstituted quinoline derivatives.

For the 5-R and 6-R quinolines, Figure 6 shows that the pK_a^* generally increases as Δq or Δq^* on the ring nitrogen becomes more negative. Indeed, linear regression analysis on the plots of pK_a^* versus Δq^* reveals R^2 values of 0.96 and 0.98 for the 5-R and 6-R quinolines. Figure S6 in the Supporting Information shows that the corresponding R^2 values for pK_a^* versus Δq are 0.89 and 0.92 for the 5-R and 6-R quinolines, respectively. This analysis demonstrates that, for a fixed substituent position, the thermodynamic driving force for excited-state protonation of the ring nitrogen is strongly correlated with the increase in the electron density on the ring nitrogen.

This suggests that the degree of charge-transfer character of the $S_0 \rightarrow S_{CT}$ transition affects the strength of the photobasicity.
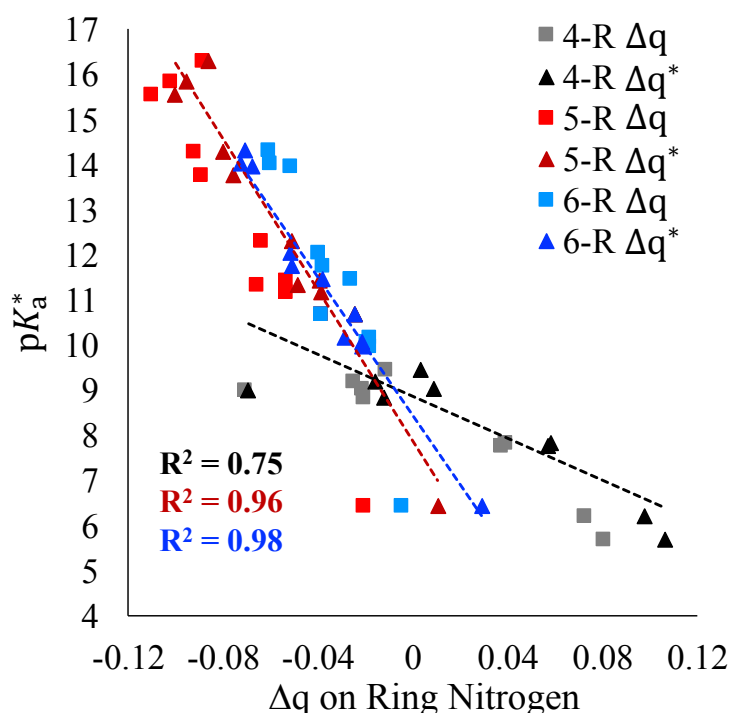

Figure 6: Plot of pK_a^* versus change in charge on the ring nitrogen for the 4-R, 5-R, and 6-R monosubstituted quinoline compounds. The change in charge on the ring nitrogen are calculated at the ground state geometry (Δq, squares) and at the excited state optimized geometry (Δq^*, triangles). The reported R^2 values are from linear regression analysis performed on the Δq^* data.

The 4-R quinoline compounds represent an interesting case because, as discussed above, they display the opposite trend as the other monosubstituted quinoline compounds. Figure 6 shows that many of these compounds have positive Δq and Δq^* on the ring nitrogen, suggesting that this atom loses electron density in the $S_0 \rightarrow S_{CT}$ transition and hence becomes less basic. Moreover, as shown in Table S3 in the Supporting Information, Δq and Δq^* become increasingly positive as the R group is made more electron-donating. This reflects the fact that Figure 5 shows that 4-aminoquinoline has a smaller pK_a^* than 4-cyanoquinoline. Finally, note that while

the 4-R quinolines exhibit the same overall trend in Figure 6 as the 5-R and 6-R quinolines, the slope is markedly smaller.

Before ending our discussion of Figure 6, we consider the magnitude of the Δq and Δq^* observed in the calculations as well as the extent to which the these quantities are predictive of pK_a^*. For all of the compounds shown in Figure 6, as well as those analyzed in Figure S6 in the Supporting Information, the magnitudes of Δq and Δq^* are modest, with the gain or loss of charge on the ring nitrogen less than 0.15 electrons. Moreover, vibrational relaxation on S_{CT} does not always lead to an increase in the magnitude of the charge-transfer; for the 6-R quinolines Δq^* is more negative than Δq while the opposite is true for the 5-R quinolines. Additionally, Figures 6 and S6 contain multiple examples of compounds which have very similar Δq and Δq^* and yet significantly different pK_a^*. This shows that, aside from the observation that all strong photobases have $\Delta q < 0$, one should not use Δq or Δq^* as a proxy for pK_a^* when predicting the photobasicity of a new compound. Moreover, the above analysis suggests that while S_{CT} should have some charge-transfer character, with the ring nitrogen gaining electron density in the $S_0 \rightarrow S_{CT}$ transition, the thermodynamic driving force of the excited state protonation of these photobases cannot be solely attributed to the build-up of excess charge on the ring nitrogen.

Finally, we briefly describe the geometric changes that result from the vibrational relaxation on S_{CT}. For all of the compounds, the excited-state geometry optimization causes a distortion to the aromatic rings which results in a modest elongation of the molecules. The most pronounced geometric changes occur with the amine substituents which, as much as sterically possible, undergo planarization during the vibrational relaxation. This is most pronounced for the basic forms of the compounds; the amine groups are often planar in the ground-state

optimized geometries of the acidic forms. Examples of this can be seen in Figures S7 and S8 in the Supporting Information for 8-aminoquinoline and 8-dimethylaminoquinoline.

Expanding the Scope of Nitrogen-Containing Aromatic Heterocyclic Photobases: Disubstituted Quinolines, Isoquinolines, Acridines, and 1-Azaanthracenes

Figure 7 summarizes the diversity of compounds we considered in this study which are identified to be strong bases in S_{CT}, $pK_a^* > 14$, along with their corresponding vertical excitation energies; the complete data set generated in this study is provided in the Supporting Information. We specifically focused on monosubstituted (squares) or disubstituted (triangles) quinoline (purple data), isoquinoline (green data), acridine (blue data), and 1-azaanthracene (red data). Because we are interested in identifying compounds with the potential for use in photocatalysis, we focused exclusively on electron-donating substituents in developing this dataset.
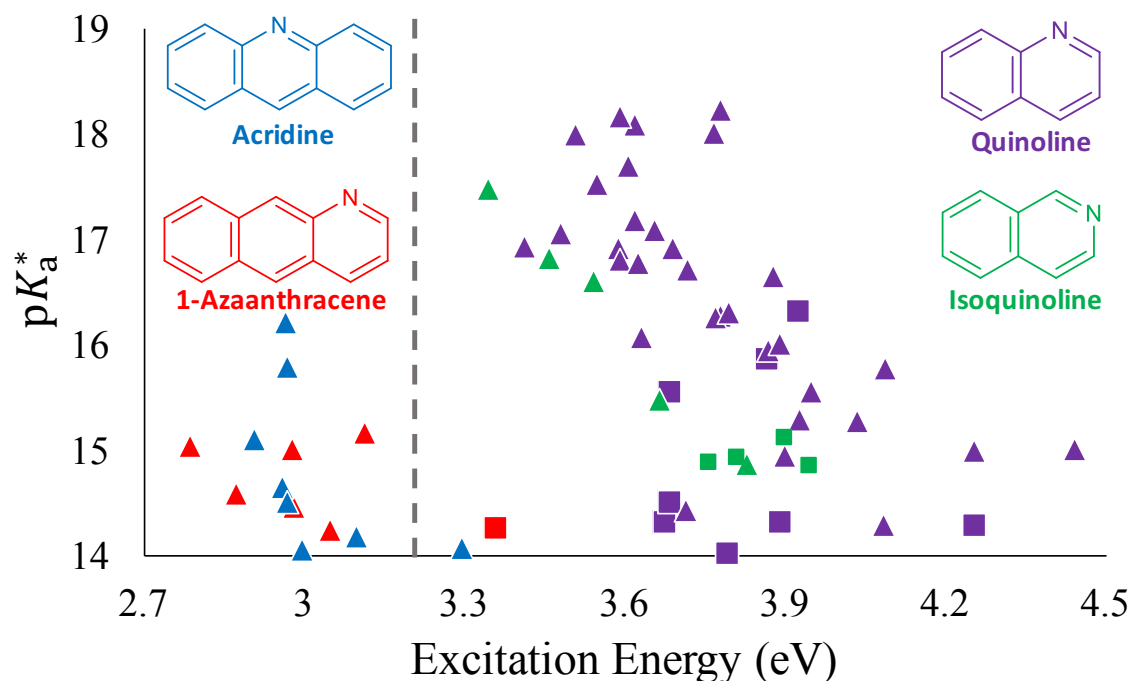
Figure 7: A plot of pK_a^* versus $S_0 \rightarrow S_{CT}$ vertical excitation energies for the compounds identified in this study to be strong bases in the excited state. The monosubstituted compounds are represented by squares while the disubstituted compounds are denoted by triangles. The dashed gray line denotes the boundary between visible (hν<3.26 eV) and UV (hν>3.26 eV) light.

Focusing first on the disubstituted quinoline derivatives, Figure 7 demonstrates that the effects of electron-donating substituents on photobasicity are additive as many of the disubstituted quinoline compounds have significantly greater pK_a^* than the monosubstituted compounds. For example, 5,6-aminoquinoline has $pK_a^* = 18.16$ whereas 5-aminoquinoline and 6-aminoquinoline have $pK_a^* = 15.85$ and $pK_a^* = 13.96$ respectively. The disubstituted compounds with the largest pK_a^* have both substituents in positions that Figure 5 identifies as being supportive of increased photobasicity. In particular, the strongest photobases have an amine group in the 5 position along with either another amine group in the 6 position or an electron-donating group in the 8 position which cannot engage in hydrogen bonding with the ring nitrogen. Tables S7-S8 in the Supporting Information further show that an electron-donating substituent in the 4 position continues to decrease the photobasicity in the disubstituted quinolines; the pK_a^* of 4,5-aminoquinoline, 13.58, is lower than that of 5-aminoquinoline, 15.85. Finally, note that Figure 7 demonstrates that, in addition to increasing pK_a^*, the presence of a second electron-donating substituent tends to result in a reduction of the vertical excitation energy. Nevertheless, all of these disubstituted quinolines are still predicted to absorb in the UV.

The isoquinoline compounds are shown in Figure 7 to follow the same overall trends as the quinoline compounds, although the isoquinoline compounds tend to have a somewhat lower pK_a^* than their quinoline counterparts. Electron-donating substituents in the 5 and 8 positions of isoquinoline (which are comparable to the 5 and 8 positions of quinoline) result in the largest pK_a^* and lowest vertical excitation energies. In particular, 8-amino-isoquinoline is the most strongly photobasic monosubstituted isoquinoline compound with $pK_a^* = 15.12$ while 5,8-amino-isoquinoline has the largest pK_a^* of the disubstitued compounds at 17.48. Note that substituents in the 8 position of isoquinoline have a purely electronic effect on the photobasicity;

because the ring nitrogen is now in position 2, there can be no hydrogen bonding or steric interactions between it and a substituent in position 8. Similar to the 4-R quinoline compounds, Table S9 in the Supporting Information shows that increasingly electron-donating substituents in the 4 position of isoquinoline reduce the photobasicity; 4-methyl-isoquinoline and 4-amino-isoquinoline have $pK_a^* = 9.23$ and $pK_a^* = 8.06$, respectively.

With the addition of a second fused benzene ring, the vertical excitation energies of the acridine and 1-azaanthracene compounds are significantly reduced relative to that of the quinoline and isoquinoline compounds, with several examples in Figure 7 having vertical excitation energies in the visible region of the spectrum (to the left of the dashed gray line). As more fully shown in Tables S10-S12 in the Supporting Information, this reduction in the vertical excitation energy is accompanied by a general decrease in pK_a^* relative to quinoline and isoquinoline. Nevertheless, Figure 7 shows 15 acridine and 1-azaanthracene derivatives with $pK_a^* > 14$, 13 of which are predicted to absorb in the visible. With the exception of 6-methylamino-1-azaanthracene, these compounds are all disubstituted with two strong electron-donating substituents. In the case of the acridine derivatives, the strongest photobases are asymmetric, with an amine in the 1 position and the other electron-donating substituent on the same fused benzene ring in either the 2 or 4 position. The strongest such photobase considered in this study is 1,2-methylaminoacridine with $pK_a^* = 16.21$. For the 1-azaanthracene compounds, the strongest photobases have the two substituents on the terminal fused benzene ring, with an amine group in the 6 position and another amine group in the 7 or 9 position. 6,9-dimethylamino-1-azaanthracene, the strongest such photobase considered in this study, has $pK_a^* = 15.17$.

The relationship between pK_a^* and the extent of charge-transfer character of S_{CT} is further explored in Figure 8 for the disubstituted quinolines, acridines, and 1-azaanthracenes. Here, we see that pK_a^* generally increases as Δq^* on the ring N becomes more negative. However, the relationship between pK_a^* and Δq^* is too noisy to allow Δq^* to definitively predict the photobasicity strength. This is especially true for the disubstituted 1-azaanthracene data where a very narrow range of relatively small Δq^* values correspond to pK_a^* ranging from 10.75 to 15.17. Figure S27 in the Supporting Information demonstrates that, for the same set of compounds, the correlation between Δq and pK_a^* is even less clear than the correlation between Δq^* and pK_a^* in Figure 8. The variability present in Figures 8 and S27 reflects, as discussed above, the fact that the thermodynamics of the excited state protonation of these compounds is not fully controlled by the degree to which the $S_0 \rightarrow S_{CT}$ transition builds up electron density on the ring nitrogen. Finally, note that the correlations between Δq and pK_a^* for the disubstituted quinoline, isoquinoline, acridine, and 1-azaanthracene compounds considered in this study are presented in Figures S13, S18, and S26 in the Supporting Information.
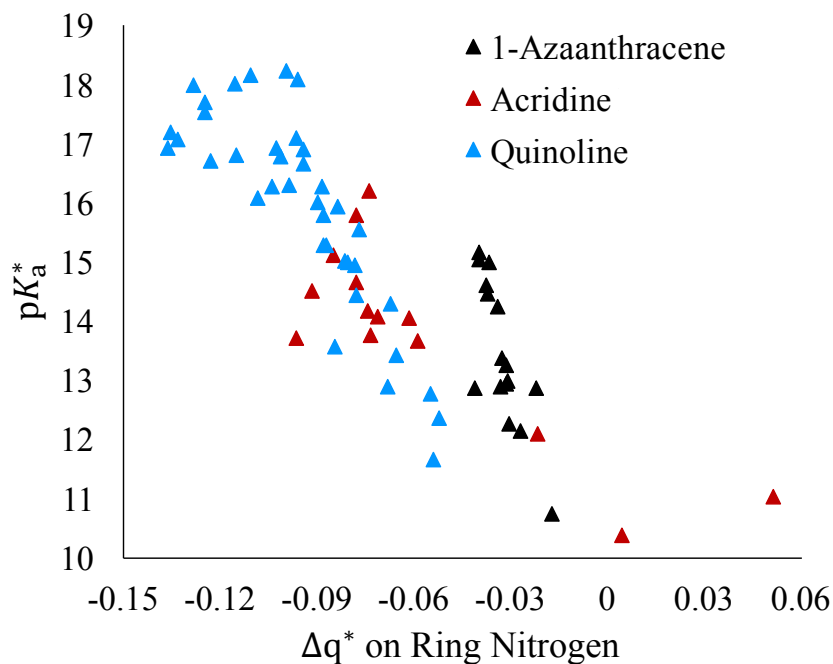
Figure 8: Plot of pK_a^* versus change in charge (Δq^*) on the ring nitrogen at the excited state optimized geometry for the disubstituted 1-azaanthracene (black), acridine (red), and quinoline (blue) compounds. Linear regression analysis leads to R^2 values of 0.63, 0.71, and 0.71 for the 1-azaanthracene, acridine, and quinoline data respectively.

On the Validity of the Förster Mechanism for Nitrogen-Containing Aromatic Heterocycles

Containing Strong Electron-Donating Groups

The analysis presented in this paper assumes that the photobasicity of nitrogen-containing heterocycles containing strong electron-donating groups is well-described by the Förster mechanism. This relies on the S_{CT} excited state having a long enough lifetime for the excited state protonation to occur prior to any non-radiative transitions to other states. Under such conditions, the trends in the photobasicity of these compounds will be well captured by the thermodynamic analysis presented above.

Using transient absorption spectroscopy, Dawlaty and coworkers identified evidence of S_{CT} undergoing intersystem crossing into the triplet manifold for a series of 5-R quinolines.[21] In particular, for 5-aminoquinoline, the strongest photobase that was experimentally investigated,

the spectroscopic evidence points to excited state protonation occurring on a timescale of 41 ps followed by relaxation into a triplet state approximately 36 ps later. Such a process does not necessarily invalidate the applicability of the Förster mechanism to the photobasicity of 5-aminoquinoline as the intersystem crossing only occurs after the excited state protonation. In contrast, for the weaker photobases quinoline, 5-chloroquinoline, 5-bromoquinoline, and 5-cyanoquinoline intersystem crossing was found to be rapid, occurring on a timescale of less than 1 ps and preceding any excited state protonation.

While a complete analysis of intersystem crossing pathways is outside the scope of the present study, we did analyze the vertical energy gap between S_{CT} and neighboring triplet states at the optimized S_{CT} geometries for representative compounds identified as strong photobases. This data, which was calculated using the Tamm-Dancoff approximation to minimize triplet instability problems, is summarized in Tables S13-S16 in the Supporting Information.[43] For the acridine and 1-azaanthracene compounds, the average $\left|E_{T_{min}} - E_{S_{CT}}\right|$ is 0.52 eV and 0.71 eV for the basic and acidic forms respectively, where T_{min} is chosen as the triplet state closest in energy to S_{CT}. T_{min} is always uphill in energy from S_{CT} for the base and often downhill in energy from S_{CT} for the acid. Similar analysis performed on the quinoline derivatives shows that the average $\left|E_{T_{min}} - E_{S_{CT}}\right|$ is 0.21 eV and 0.51 eV for the basic and acidic forms. In particular, the T_{min} of 6-aminoquinoline, 6-methylaminoquinoline, 6-dimethylaminoquinoline, 3,5-aminoquinoline, and 3,5-dimethylaminoquinoline is within 0.16 eV of S_{CT} and downhill in energy from it, suggesting a potential non-radiative relaxation pathway that could compete with excited state protonation for these five compounds. For the other quinoline derivatives, the closest triplet state is uphill in energy from S_{CT} by 0.10-0.42 eV for the basic form, suggesting that intersystem crossing may be less important for these compounds, at least prior to protonation. We stress, though, that the

analysis presented here is only preliminary and that a more complete picture of the intersystem crossing pathways in these photobases will represent an important addition to the thermodynamic trends presented in this paper. Efforts to accomplish this are currently underway.

A recent computational study by the Furche group argues for an alternative mechanism for the photobasisicity of 5-methoxyquinoline in which the S_{CT} state undergoes internal conversion into a dark singlet state with significant intermolecular charge-transfer character from a solvent water molecule to the photobase.[44] This results in the transient photooxidation of the solvent water molecule, producing a 5-methoxyquinoline radical anion and H_2O radical cation pair stabilized by the exciton binding energy. Subsequent proton transfer followed by back-electron transfer ultimately generates protonated 5-methoxyquinoline in the ground state and hydroxide. By comparing the calculated excited state electron affinity of 5-methoxyquinoline to the estimated 6.5±0.5 eV ionization potential of H_2O, Furche and coworkers arrive at a lower bound to the exciton binding energy of 0.7±0.5 eV.[45]

In Table 1, we report the excited state electron affinity of representative compounds considered in this study, calculated as the difference in the electronic energy of S_{CT} and the radical anion ($E_{radical\ anion} - E_{S_{CT}}$) at the S_{CT} optimized geometry. The radical anion is described using the restricted open-shell formalism to eliminate spin contamination. As shown in Table 1, in going from 5-methoxyquinoline to 5-aminoquinoline the $E_{radical\ anion} - E_{S_{CT}}$ decreases in magnitude by over 0.5 eV from -5.63 eV to -5.11 eV. The excited state electron affinity is even smaller in magnitude when a second electron-donating group is added, $E_{radical\ anion} - E_{S_{CT}}$ = -4.53 eV for 5,6-aminoquinoline, -4.53 eV for 1,2-aminoacridine, and -4.51 eV for 6,7-amino-1-azaanthracene.

Table 1 also reports the energy difference between S_{CT} and the intermolecular charge transfer state involving the solvent water molecule that is hydrogen bonding with the photobase, $S_{CT\,H_2O}$, at optimized geometries on S_0 and S_{CT}. These calculations were performed with four explicit water molecules forming a hydrogen bonding network around the ring nitrogen, the same model as used by Furche and coworkers. At both the S_0 and S_{CT} geometries, $E_{S_{CT\,H_2O}} - E_{S_{CT}}$ increases as the substituent is made more electron-donating. The addition of a second amine group results in a further increase in the energy gap, raising $E_{S_{CT\,H_2O}} - E_{S_{CT}}$ to over 1.3 eV and 2.2 eV at the S_0 and S_{CT} optimized geometries, respectively. Finally, for all of the compounds, relaxation on S_{CT} results in an increase in $E_{S_{CT\,H_2O}} - E_{S_{CT}}$.

Table 1: Calculated exited state electron affinities ($E_{\text{radical anion}} - E_{S_{CT}}$) and $E_{S_{CT\,H_2O}} - E_{S_{CT}}$ energy gaps for a range of nitrogen-containing heterocyclic compounds.

Compound	$E_{\text{radical anion}} - E_{S_{CT}}$ (eV)	$E_{S_{CT\,H_2O}} - E_{S_{CT}}$ S_0 Geometry (eV)[47]	$E_{S_{CT\,H_2O}} - E_{S_{CT}}$ S_{CT} Geometry (eV)[47]
5-chloroquinoline	−6.21	0.25	0.66
quinoline	−6.21	0.08	0.45
5-methylquinoline	−5.99	0.28	0.73
5-methoxyquinoline	−5.63	0.68	1.22
5-aminoquinoline	−5.11	1.07	1.72
5-dimethylaminoquinoline	−5.09	1.02	1.68
5,6-aminoquinoline	−4.53	1.37	2.23
1,2-aminoacridine	−4.53	1.57	2.26
6,7-amino-1-azaanthracene[46]	−4.51	1.59	2.23

The analysis reported in Table 1 suggests that as the strength and number of electron-donating substituents increases, the photooxidative mechanism becomes less favorable in two ways. First, the major component of the thermodynamic driving force for the solvent to solute charge-transfer, the excited state electron affinity of the photobase, is reduced by over 1 eV from

5-methoxyquinoline to the disubstituted compounds. Second, the two states involved in the photooxidation mechanism, S_{CT} and $S_{CT\,H_2O}$, grow further apart in energy as the substituents are made increasingly electron-donating. This energy gap is important because the photooxidative mechanism relies on the existence of a thermally accessible conical intersection between S_{CT} and $S_{CT\,H_2O}$, which becomes less likely as $E_{S_{CT\,H_2O}} - E_{S_{CT}}$ increases. Moreover, this energy gap significantly increases with vibrational relaxation on S_{CT}. It is therefore reasonable to conclude that the photooxidative mechanism becomes less likely as the electron-donating strength of the substituent(s) increases.

Conclusions

Overall, the results reported in this study demonstrate the degree to which two key properties of photobases, pK_a^* and the excitation energy, can be tuned for quinoline and related compounds through substituents. We demonstrated that the photobasicity is affected by the identity, quantity, and position of the substituent(s). We showed that the addition of a second electron-donating substituent to quinoline can result in a significant increase in pK_a^* relative to the monosubstituted quinoline compounds. We identified a number of disubstituted acridine and 1-azaanthracene compounds with vertical excitation energies under 3.1 eV and $pK_a^* > 14$. The structure-function relationships uncovered in this study therefore provide insights into the design principles needed for the development of new photocatalysts which incorporate photobasicity. Efforts to extend this analysis to more complex nitrogen-containing heterocyclic aromatics containing multiple heteroatoms as well as to more rigorously explore the impact of other photochemical pathways (e.g. intersystem crossing) on the photobasicity of the compounds considered in this study are currently underway in our lab.

Supporting Information

The complete dataset analyzed in this study, images of the HONTO and LUNTO for representative compounds, plots illustrating the correlation between pK_a^* and Δq on the ring N, and analysis of energy differences between S_{CT} and neighboring triplet states are provided in the Supporting Information.

References

(1)   Tolbert, L. M.; Solntsev, K. M. Excited-State Proton Transfer: From Constrained Systems to "Super" Photoacids to Superfast Proton Transfer. *Acc. Chem. Res.* **2002**, *35* (1), 19–27. https://doi.org/10.1021/ar990109f.

(2)   Zhou, P.; Han, K. Unraveling the Detailed Mechanism of Excited-State Proton Transfer. *Acc. Chem. Res.* **2018**, *51* (7), 1681–1690. https://doi.org/10.1021/acs.accounts.8b00172.

(3)   Lennox, J. C.; Kurtz, D. A.; Huang, T.; Dempsey, J. L. Excited-State Proton-Coupled Electron Transfer: Different Avenues for Promoting Proton/Electron Movement with Solar Photons. *ACS Energy Lett.* **2017**, *2* (5), 1246–1256. https://doi.org/10.1021/acsenergylett.7b00063.

(4)   Spry, D. B.; Fayer, M. D. Charge Redistribution and Photoacidity: Neutral versus Cationic

Photoacids. *J. Chem. Phys.* **2008**, *128* (8). https://doi.org/10.1063/1.2825297.

(5)   Granucci, G.; Hynes, J. T.; Millié, P.; Tran-Thi, T.-H. A Theoretical Investigation of

Excited-State Acidity of Phenol and Cyanophenols. *J. Am. Chem. Soc.* **2000**, *122* (49),

12243–12253. https://doi.org/10.1021/ja993730j.

(6)   Solntsev, K. M.; Huppert, D.; Tolbert, L. M.; Agmon, N. Solvatochromic Shifts of

"super" Photoacids [5]. *J. Am. Chem. Soc.* **1998**, *120* (31), 7981–7982.

https://doi.org/10.1021/ja9808604.

(7)   Ditkovich, J.; Mukra, T.; Pines, D.; Huppert, D.; Pines, E. Bifunctional Photoacids:

Remote Protonation Affecting Chemical Reactivity. *J. Phys. Chem. B* **2015**, *119* (6),

2690–2701. https://doi.org/10.1021/jp509104x.

(8)   Simkovitch, R.; Shomer, S.; Gepshtein, R.; Huppert, D. How Fast Can a Proton-Transfer

Reaction Be beyond the Solvent-Control Limit? *J. Phys. Chem. B* **2015**, *119* (6), 2253–

2262. https://doi.org/10.1021/jp506011e.

(9)   Simkovitch, R.; Karton-lifshin, N.; Shomer, S.; Shabat, D.; Huppert, D. Ultrafast Excited-

State Proton Transfer to the Solvent Occurs on a Hundred-Femtosecond Time-Scale.

2013. https://doi.org/10.1021/jp4014724.

(10)   Agmon, N. Elementary Steps in Excited-State Proton Transfer †. *J. Phys. Chem. A* **2005**,

109 (1), 13–35. https://doi.org/10.1021/jp047465m.

(11)   Cotter, L. F.; Brown, P. J.; Nelson, R. C.; Takematsu, K. Divergent Hammett Plots of the

Ground- and Excited-State Proton Transfer Reactions of 7-Substituted-2-Naphthol

Compounds. *J. Phys. Chem. B* **2019**, *123* (19), 4301–4310.

https://doi.org/10.1021/acs.jpcb.9b01295.

(12)   Favaro, G.; Mazzucato, U.; Masetti, F. Excited State Reactivity of Aza Aromatics. I.

Basicity of 3-Styrylpyridines in the First Excited Singlet State. *J. Phys. Chem.* **1973**, *77* (5), 601–604. https://doi.org/10.1021/j100624a007.

(13)   Pines, E.; Huppert, D.; Gutman, M.; Nachliel, N.; Fishman, M. The POH Jump: Determination of Deprotonation Rates of Water by 6-Methoxyquinoline and Acridine. *J. Phys. Chem.* **1986**, *90* (23), 6366–6370. https://doi.org/10.1021/j100281a061.

(14)   Nachliel, E.; Ophir, Z.; Gutman, M. Kinetic Analysis of Fast Alkalinization Transient by Photoexcited Heterocyclic Compounds: POH Jump. *J. Am. Chem. Soc.* **1987**, *109* (5), 1342–1345. https://doi.org/10.1021/ja00239a009.

(15)   Solntsev, K. M.; Sullivan, E. N.; Tolbert, L. M.; Ashkenazi, S.; Leiderman, P.; Huppert, D. Excited-State Proton Transfer Reactions of 10-Hydroxycamptothecin 1. *J. Am. Chem. Soc.* **2004**, *126* (39), 12701–12708. https://doi.org/10.1021/ja047821e.

(16)   Akulov, K.; Simkovitch, R.; Erez, Y.; Gepshtein, R.; Schwartz, T.; Huppert, D. Acid Effect on Photobase Properties of Curcumin. *J. Phys. Chem. A* **2014**, *118* (13), 2470–2479. https://doi.org/10.1021/jp501061p.

(17)   Poizat, O.; Bardez, E.; Buntinx, G.; Alain, V. Picosecond Dynamics of the Photoexcited 6-Methoxyquinoline and 6-Hydroxyquinoline Molecules in Solution. *J. Phys. Chem. A* **2004**, *108* (11), 1873–1880. https://doi.org/10.1021/jp030964n.

(18)   Yatsuhashi, T.; Inoue, H. Molecular Mechanism of Radiationless Deactivation of Aminoanthraquinones through Intermolecular Hydrogen-Bonding Interaction with Alcohols and Hydroperoxides. *J. Phys. Chem. A* **1997**, *101* (44), 8166–8173. https://doi.org/10.1021/jp970581n.

(19)   Sheng, W.; Nairat, M.; Pawlaczyk, P. D.; Mroczka, E.; Farris, B.; Pines, E.; Geiger, J. H.; Borhan, B.; Dantus, M. Ultrafast Dynamics of a "Super" Photobase. *Angew. Chemie Int.*

Ed. **2018**, *57* (45), 14742–14746. https://doi.org/10.1002/anie.201806787.

(20) Driscoll, E. W.; Hunt, J. R.; Dawlaty, J. M. Photobasicity in Quinolines: Origin and

Tunability via the Substituents' Hammett Parameters. *J. Phys. Chem. Lett.* **2016**, *7* (11),

2093–2099. https://doi.org/10.1021/acs.jpclett.6b00790.

(21) Driscoll, E. W.; Hunt, J. R.; Dawlaty, J. M. Proton Capture Dynamics in Quinoline

Photobases: Substituent Effect and Involvement of Triplet States. *J. Phys. Chem. A* **2017**,

121, 7099–7107. https://doi.org/10.1021/acs.jpca.7b04512.

(22) Hunt, J. R.; Dawlaty, J. M. Photodriven Deprotonation of Alcohols by a Quinoline

Photobase. *J. Phys. Chem. A* **2018**, *122* (40), 7931–7940.

https://doi.org/10.1021/acs.jpca.8b06152.

(23) Demianets, I.; Hunt, J. R.; Dawlaty, J. M.; Williams, T. J. Optical PK$_a$ Control in a

Bifunctional Iridium Complex. *Organometallics* **2019**, *38* (2), 200–204.

https://doi.org/10.1021/acs.organomet.8b00778.

(24) Hunt, J. R.; Tseng, C.; Dawlaty, J. M. Donor–Acceptor Preassociation, Excited State

Solvation Threshold, and Optical Energy Cost as Challenges in Chemical Applications of

Photobases. *Faraday Discuss.* **2019**, *00*, 1–17. https://doi.org/10.1039/c8fd00215k.

(25) Hunt, J. R.; Dawlaty, J. M. Kinetic Evidence for the Necessity of Two Proton Donor

Molecules for Successful Excited State Proton Transfer by a Photobase. *J. Phys. Chem. A*

2019, *123* (48), 10372–10380. https://doi.org/10.1021/acs.jpca.9b08970.

(26) Chai, J.-D.; Head-Gordon, M. Long-Range Corrected Hybrid Density Functionals with

Damped Atom–Atom Dispersion Corrections. *Phys. Chem. Chem. Phys.* **2008**, *10* (44),

6615. https://doi.org/10.1039/b810189b.

(27) Chai, J.-D.; Head-Gordon, M. Systematic Optimization of Long-Range Corrected Hybrid

Density Functionals. *J. Chem. Phys.* **2008**, *128* (8), 084106.
https://doi.org/10.1063/1.2834918.

(28) Tomasi, J.; Mennucci, B.; Cammi, R. Quantum Mechanical Continuum Solvation Models.
Chem. Rev. **2005**, *105* (8), 2999–3094. https://doi.org/10.1021/cr9904009.

(29) Lange, A. W.; Herbert, J. M. A Smooth, Nonsingular, and Faithful Discretization Scheme
for Polarizable Continuum Models: The Switching/Gaussian Approach. *J. Chem. Phys.*
2010, *133* (24), 244111. https://doi.org/10.1063/1.3511297.

(30) Lange, A. W.; Herbert, J. M. Polarizable Continuum Reaction-Field Solvation Models
Affording Smooth Potential Energy Surfaces. *J. Phys. Chem. Lett.* **2010**, *1* (2), 556–561.
https://doi.org/10.1021/jz900282c.

(31) Shao, Y.; Gan, Z.; Epifanovsky, E.; Gilbert, A. T. B.; Wormit, M.; Kussmann, J.; Lange,
A. W.; Behn, A.; Deng, J.; Feng, X.; et al. Advances in Molecular Quantum Chemistry
Contained in the Q-Chem 4 Program Package. *Mol. Phys.* **2015**, *113* (2), 184–215.
https://doi.org/10.1080/00268976.2014.952696.

(32) Cordova, F.; Doriol, L. J.; Ipatov, A.; Casida, M. E.; Filippi, C.; Vela, A. Troubleshooting
Time-Dependent Density-Functional Theory for Photochemical Applications: Oxirane. *J.
Chem. Phys.* **2007**, *127* (16), 164111. https://doi.org/10.1063/1.2786997.

(33) Mewes, J.-M.; You, Z.-Q.; Wormit, M.; Kriesche, T.; Herbert, J. M.; Dreuw, A.
Experimental Benchmark Data and Systematic Evaluation of Two a Posteriori ,
Polarizable-Continuum Corrections for Vertical Excitation Energies in Solution. *J. Phys.
Chem. A* **2015**, *119* (21), 5446–5464. https://doi.org/10.1021/jp511163y.

(34) You, Z.-Q.; Mewes, J.-M.; Dreuw, A.; Herbert, J. M. Comparison of the Marcus and
Pekar Partitions in the Context of Non-Equilibrium, Polarizable-Continuum Solvation

Models. *J. Chem. Phys.* **2015**, *143* (20), 204104. https://doi.org/10.1063/1.4936357.

(35) Rohrdanz, M. A.; Martins, K. M.; Herbert, J. M. A Long-Range-Corrected Density

Functional That Performs Well for Both Ground-State Properties and Time-Dependent

Density Functional Theory Excitation Energies, Including Charge-Transfer Excited States.

J. Chem. Phys. **2009**, *130* (5), 054112. https://doi.org/10.1063/1.3073302.

(36) Prlj, A.; Sandoval-Salinas, M. E.; Casanova, D.; Jacquemin, D.; Corminboeuf, C. Low-

Lying Ππ* States of Heteroaromatic Molecules: A Challenge for Excited State Methods.

J. Chem. Theory Comput. **2016**, *12* (6), 2652–2660.

https://doi.org/10.1021/acs.jctc.6b00245.

(37) Kohn, A. W.; Lin, Z.; Van Voorhis, T. Toward Prediction of Nonradiative Decay

Pathways in Organic Compounds I: The Case of Naphthalene Quantum Yields. *J. Phys.

Chem. C* **2019**, *123* (25), 15394–15402. https://doi.org/10.1021/acs.jpcc.9b01243.

(38) Martin, R. L. Natural Transition Orbitals. *J. Chem. Phys.* **2003**, *118* (11), 4775–4777.

https://doi.org/10.1063/1.1558471.

(39) Plasser, F.; Wormit, M.; Dreuw, A. New Tools for the Systematic Analysis and

Visualization of Electronic Excitations. I. Formalism. *J. Chem. Phys.* **2014**, *141* (2),

024106. https://doi.org/10.1063/1.4885819.

(40) Closser, K. D.; Gessner, O.; Head-Gordon, M. Simulations of the Dissociation of Small

Helium Clusters with Ab Initio Molecular Dynamics in Electronically Excited States. *J.

Chem. Phys.* **2014**, *140* (13), 134306. https://doi.org/10.1063/1.4869193.

(41) Brown, H. C.; Okamoto, Y. Electrophilic Substituent Constants. *J. Am. Chem. Soc.* **1958**,

80 (18), 4979–4987. https://doi.org/10.1021/ja01551a055.

(42) Leffler, J. E.; Grunwald, E. *Rates and Equilibria of Organic Reactions: As Treated by*

Statistical, Thermodynamic and Extrathermodynamic Methods; John Wiley & Sons, Inc.: New York, 1963.

(43)   Peach, M. J. G.; Williamson, M. J.; Tozer, D. J. Influence of Triplet Instabilities in TDDFT. *J. Chem. Theory Comput.* **2011**, *7* (11), 3578–3585. https://doi.org/10.1021/ct200651r.

(44)   Roy, S.; Ardo, S.; Furche, F. 5-Methoxyquinoline Photobasicity Is Mediated by Water Oxidation. *J. Phys. Chem. A* **2019**, *123* (31), 6645–6651. https://doi.org/10.1021/acs.jpca.9b05341.

(45)   Bernas, A.; Grand, D. The So-Called Ionization Potential of Water and Associated Liquids. *J. Phys. Chem.* **1994**, *98* (13), 3440–3443. https://doi.org/10.1021/j100064a027.

(46)   The reported data is from an optimized geometry with a single imaginary vibrational frequency of 28.14i cm^{-1}. We were unable to obtain a better optimized geometry for this complex.

(47)   The electronic excited states were obtained using the Tamm-Dancoff approximation because of numerical issues that arose when calculating the full TD-DFT energies for some of these complexes.

TOC Graphic
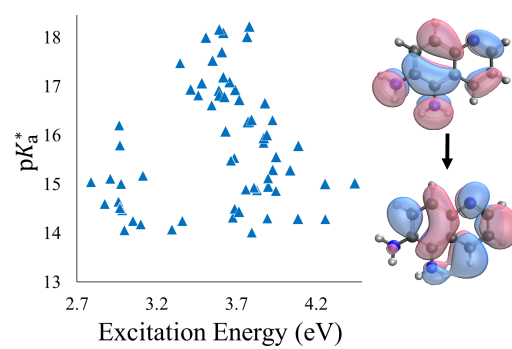
Supporting Information for "Structure-Photochemical Function Relationships in Nitrogen-Containing Heterocyclic Aromatic Photobases Derived from Quinoline"

Sophya F. Alamudun, Kyle Tanovitz, April Fajardo, Kaitlind Johnson, Andy Pham,

Tina Jamshidi Araghi, and Andrew S. Petit*

Department of Chemistry and Biochemistry, California State University, Fullerton, California

92834-6866, United States

*Corresponding author: apetit@fullerton.edu
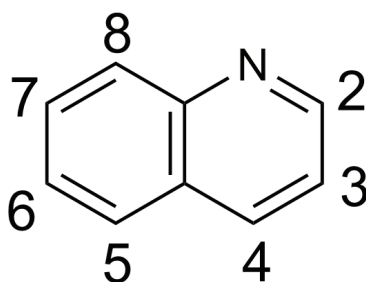
Table of Contents

Figure S1: Substituent position numbering system for the substituted quinoline compounds.

Table S1: Calculated ground state pK_a, excited state pK_a^*, vertical excitation energy, oscillator strength, and change in charge on the ring nitrogen at the ground-state (Δq) and excited-state (Δq^*) optimized geometries for the 5-R substituted quinoline compounds. The reported data is for the lowest energy $\pi \rightarrow \pi^*$ bright state with significant charge-transfer character, S_{CT}. The molecules are arranged from most electron-withdrawing substituent to most electron-donating substituent in terms of the Hammett σ_{para}^+. Where available, the experimental pK_a^* determined by Dawlaty and coworkers are provided in the right-most column.[1]

Substituent	Excitation Energy (eV)	Oscillator Strength	Δq on Ring N	Δq^* on Ring N	pK_a	pK_a^*	Experimental pK_a^*
CN	4.51	0.19	−0.021	0.010	3.22	6.43	5.4
Br	4.51	0.15	−0.054	−0.039	3.79	11.42	11.2
Cl	4.52	0.13	−0.054	−0.039	3.83	11.18	9.7
F	4.57	0.080	−0.066	−0.049	3.98	11.35	—
H	4.70	0.077	−0.039	−0.025	4.69	10.70	11.5
CH$_3$	4.52	0.11	−0.064	−0.051	4.85	12.29	—
OCH$_3$	4.26	0.12	−0.093	−0.080	4.86	14.29	15.1
OH	4.26	0.097	−0.089	−0.076	4.78	13.76	—
NH$_2$	3.87	0.12	−0.102	−0.096	5.39	15.85	15.9
N(CH$_3$)$_2$	3.93	0.14	−0.089	−0.086	4.94	16.31	—
NHCH$_3$	3.69	0.15	−0.110	−0.101	5.33	15.54	—

Table S2: Calculated ground state pK_a, excited state pK_a^*, vertical excitation energy, oscillator strength, and change in charge (Δq) on the ring nitrogen for the 3-R substituted quinoline compounds. The reported data is for the lowest energy $\pi\rightarrow\pi^*$ bright state with significant charge-transfer character, S_{CT}.

Substituent	Excitation Energy (eV)	Oscillator Strength	Δq on Ring N	pK_a	pK_a^*
CN	4.54	0.12	−0.052	2.36	7.61
Br	4.48	0.093	−0.073	3.11	10.71
Cl	4.50	0.086	−0.071	3.08	10.51
F	4.53	0.081	−0.071	3.12	10.68
CH$_3$	4.57	0.076	−0.053	4.83	9.94
OCH$_3$	4.32	0.11	−0.089	3.98	11.86
OH	4.31	0.11	−0.084	4.04	11.25
NH$_2$	3.98	0.13	−0.103	4.69	12.96
N(CH$_3$)$_2$	3.69	0.15	−0.119	4.71	14.50
NHCH$_3$	3.73	0.15	−0.108	5.01	13.40

Table S3: Calculated ground state pK_a, excited state pK_a^*, vertical excitation energy, oscillator strength, and change in charge on the ring nitrogen at the ground-state (Δq) and excited-state (Δq^*) optimized geometries for the 4-R substituted quinoline compounds. The reported data is for the lowest energy $\pi\rightarrow\pi^*$ bright state with significant charge-transfer character, S_{CT}. For the 4-OCH$_3$, 4-OH, 4-NH$_2$, and 4-NHCH$_3$ compounds, the chosen state has the least positive Δq on the ring N of the low-lying $\pi\rightarrow\pi^*$ states.

Substituent	Excitation Energy (eV)	Oscillator Strength	Δq on Ring N	Δq^* on Ring N	pK_a	pK_a^*
CN	4.25	0.12	−0.071	−0.069	2.45	8.99
Br	4.55	0.13	−0.025	−0.016	3.78	9.20
Cl	4.57	0.11	−0.021	−0.012	3.86	8.85
F	4.73	0.076	−0.021	0.008	4.26	9.02
CH$_3$	4.67	0.11	−0.012	0.003	5.22	9.45
OCH$_3$	4.65	0.14	0.037	0.057	5.89	7.78
OH	4.64	0.10	0.039	0.058	5.82	7.84
NH$_2$	4.33	0.19	0.080	0.106	7.28	5.69
NHCH$_3$	4.28	0.24	0.072	0.098	7.55	6.22

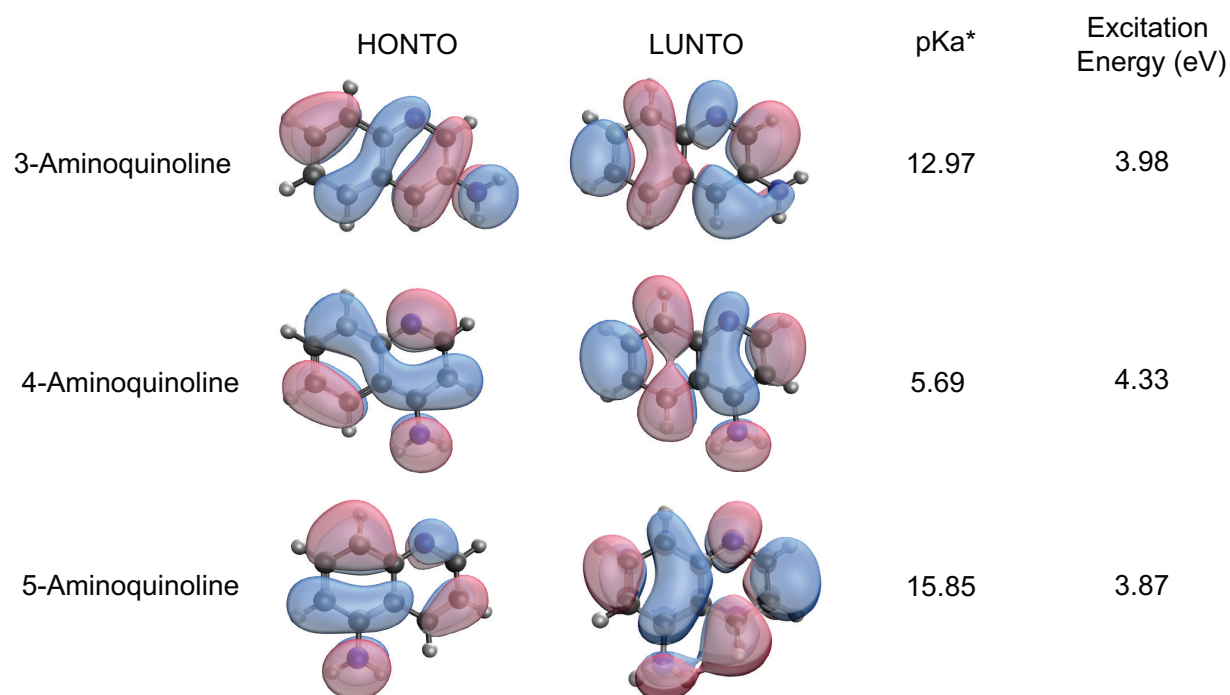|	HONTO	LUNTO	pKa*	Excitation Energy (eV)
3-Aminoquinoline			12.97	3.98
4-Aminoquinoline			5.69	4.33
5-Aminoquinoline			15.85	3.87

Figure S2: The highest occupied natural transition orbital (HONTO) and lowest unoccupied natural transition orbital (LUNTO) at the excited state optimized geometry, along with the pK_a^* and vertical excitation energy, for 3-aminoquinoline, 4-aminoquinoline, and 5-aminoquinoline. The HONTOs and LUNTOs are plotted with an isovalue of 0.06.

Table S4: Calculated ground state pK_a, excited state pK_a^*, vertical excitation energy, oscillator strength, and change in charge on the ring nitrogen at the ground-state (Δq) and excited-state (Δq^*) optimized geometries for the 6-R substituted quinoline compounds. The reported data is for the lowest energy $\pi \rightarrow \pi^*$ bright state with significant charge-transfer character, S_{CT}.

Substituent	Excitation Energy (eV)	Oscillator Strength	Δq on Ring N	Δq^* on Ring N	pK_a	pK_a^*
CN	4.48	0.034	−0.0048	0.029	3.47	6.44
Br	4.54	0.075	−0.019	−0.021	4.00	10.07
Cl	4.55	0.071	−0.018	−0.022	4.03	9.98
F	4.56	0.075	−0.019	−0.029	4.20	10.18
CH_3	4.55	0.065	−0.026	−0.038	4.88	11.46
OCH_3	4.18	0.12	−0.040	−0.052	4.77	12.03
OH	4.29	0.10	−0.038	−0.051	4.78	11.76
NH_2	3.94	0.12	−0.052	−0.068	5.36	13.96
$N(CH_3)_2$	3.68	0.13	−0.061	−0.071	5.31	14.32
$NHCH_3$	3.80	0.12	−0.060	−0.072	5.17	14.01

Table S5: Calculated ground state pK_a, excited state pK_a^*, vertical excitation energy, oscillator strength, and change in charge (Δq) on the ring nitrogen for the 7-R substituted quinoline compounds. The reported data is for the lowest energy $\pi \rightarrow \pi^*$ bright state with significant charge-transfer character, S_{CT}.

Substituent	Excitation Energy (eV)	Oscillator Strength	Δq on Ring N	pK_a	pK_a^*
CN	4.66	0.16	−0.034	3.25	7.50
Br	4.55	0.098	−0.040	4.00	10.28
Cl	4.56	0.089	−0.039	4.05	9.76
F	4.58	0.089	−0.042	4.30	9.83
CH$_3$	4.56	0.082	−0.050	5.01	11.05
OCH$_3$	4.22	0.14	−0.057	5.25	10.98
OH	4.31	0.12	−0.053	5.19	10.72
NH$_2$	3.99	0.15	−0.059	6.21	11.81
N(CH$_3$)$_2$	3.75	0.18	−0.064	6.30	12.13
NHCH$_3$	3.73	0.18	−0.060	6.11	11.42

Table S6: Calculated ground state pK_a, excited state pK_a^*, vertical excitation energy, oscillator strength, and change in charge (Δq) on the ring nitrogen for the 8-R substituted quinoline compounds. The reported data is for the lowest energy $\pi \rightarrow \pi^*$ bright state with significant charge-transfer character, S_{CT}.

Substituent	Excitation Energy (eV)	Oscillator Strength	Δq on Ring N	pK_a	pK_a^*
CN	4.59	0.12	−0.014	2.46	4.51
Br	4.50	0.14	−0.043	3.56	9.81
Cl	4.52	0.12	−0.042	3.62	9.90
F	4.57	0.074	−0.058	3.60	10.73
CH$_3$	4.54	0.10	−0.059	4.73	11.49
OCH$_3$	4.28	0.11	−0.093	5.05	13.84
OH	4.20	0.080	−0.100	3.62	10.80
NH$_2$	3.85	0.10	−0.117	3.83	12.57
N(CH$_3$)$_2$	3.89	0.14	−0.099	5.26	14.31
NHCH$_3$	3.70	0.12	−0.126	3.46	12.26
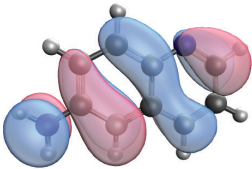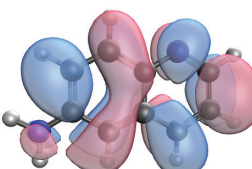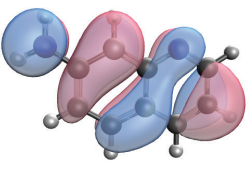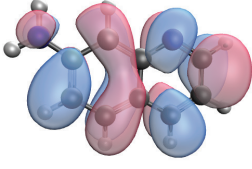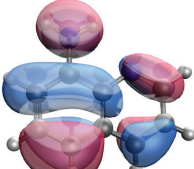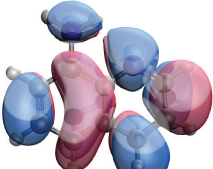
	HONTO	LUNTO	pKa*	Excitation Energy (eV)
6-Aminoquinoline			13.96	3.94
7-Aminoquinoline			11.81	3.99
8-Aminoquinoline			12.57	3.85

Figure S3: The highest occupied natural transition orbital (HONTO) and lowest unoccupied natural transition orbital (LUNTO) at the excited state optimized geometry, along with the pK_a^* and vertical excitation energy, for 6-aminoquinoline, 7-aminoquinoline, and 8-aminoquinoline. The HONTOs and LUNTOs are plotted using an isolvalue of 0.06.
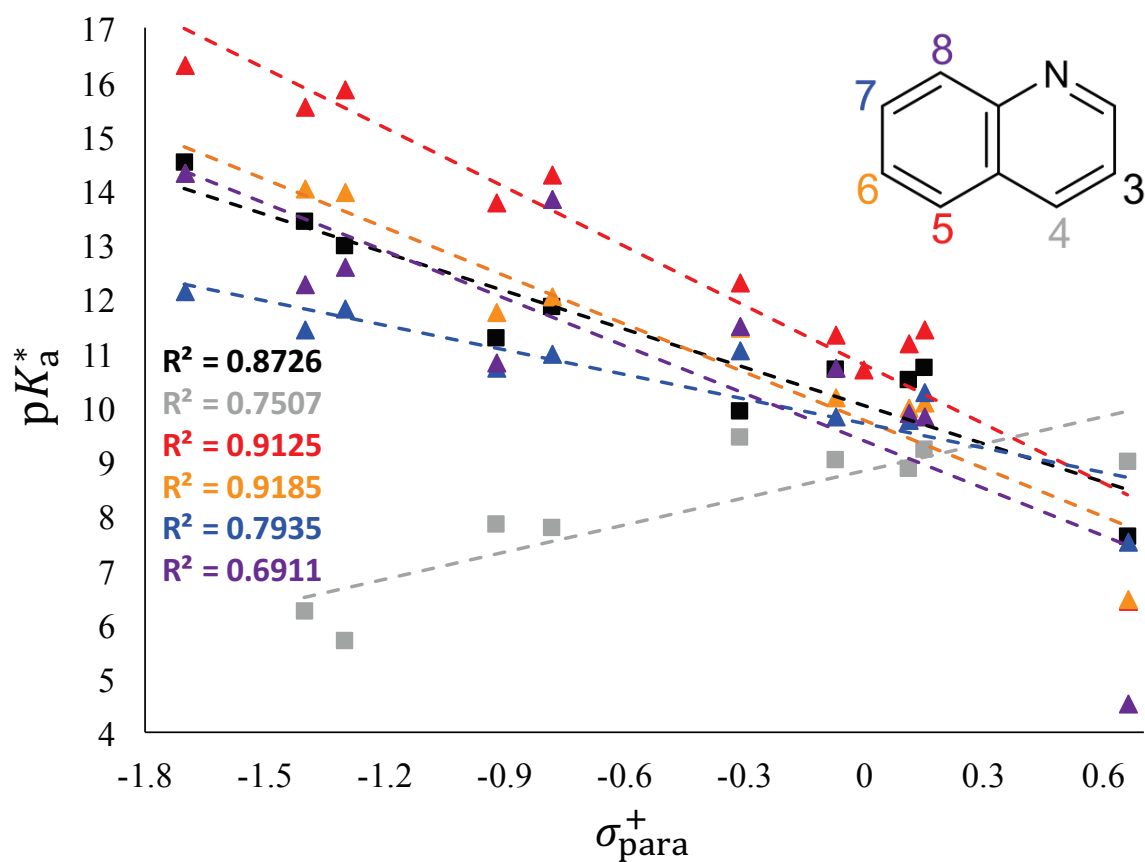
Figure S4: Calculated pK_a^* versus the Hammett σ_{para}^+ parameter of the substituent for the monosubstituted quinoline compounds considered in this study.
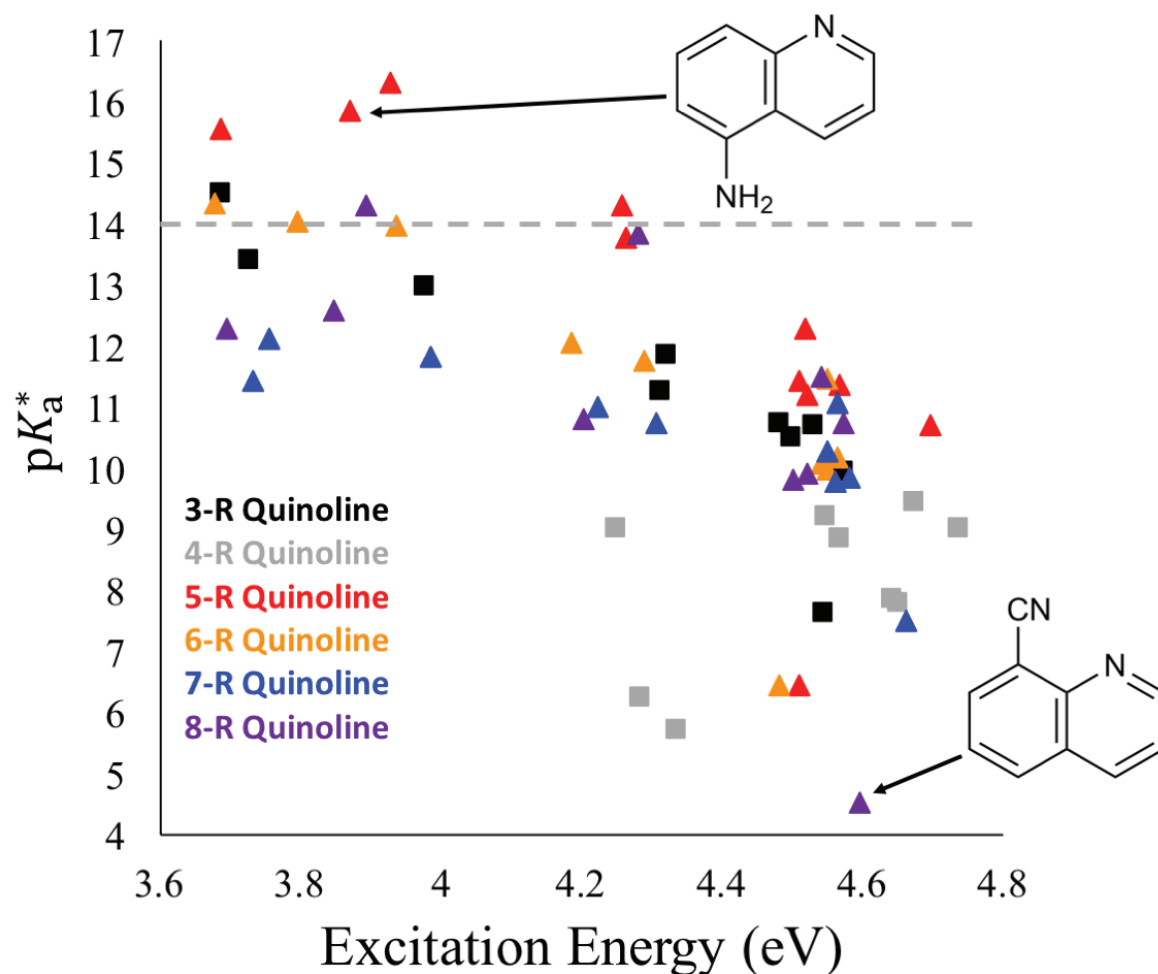
Figure S5: Plot of pK_a^* versus vertical excitation energy for all monosubstituted quinoline compounds. The squares represent compounds where the substituent is on the nitrogen-containing ring whereas the triangles represent compounds with the substituent on the fused benzene ring. Recall that all compounds with $pK_a^* > 14$ are strong bases in the excited state.
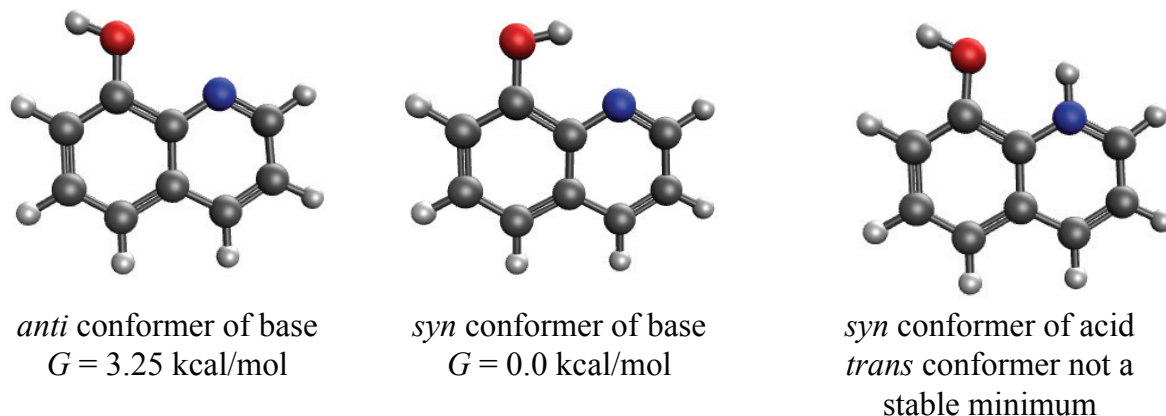
anti conformer of base
$G = 3.25$ kcal/mol

syn conformer of base
$G = 0.0$ kcal/mol

syn conformer of acid
trans conformer not a
stable minimum

Figure S6: Optimized geometries on S_0 of the base and conjugate acid forms of 8-hydroxyquinoline. While both *syn* and *anti* conformers exist for the base, only the *trans* conformer is a stable minimum for the conjugate acid. The *syn* conformer of the base is 3.25 kcal/mol lower in free energy than the *trans* conformer.
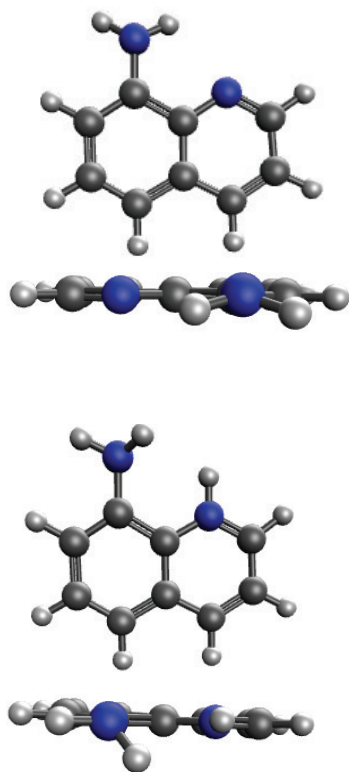
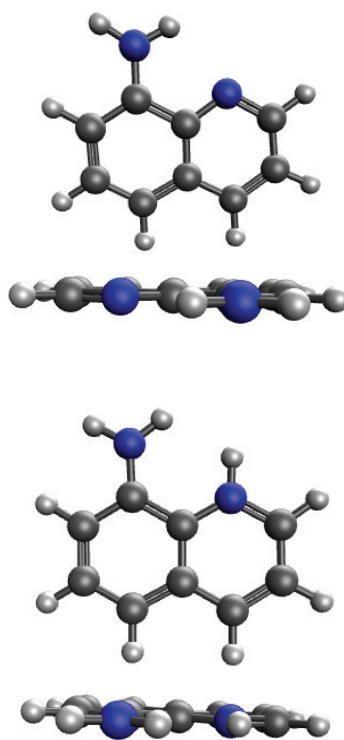S_0 Optimized Geometry S_{CT} Optimized Geometry

Figure S7: Optimized geometries on S_0 and S_{CT} for the acidic and basic forms of 8-aminoquinoline. Note that the major consequence of the excited state geometry optimization is the planarization of the amine group.
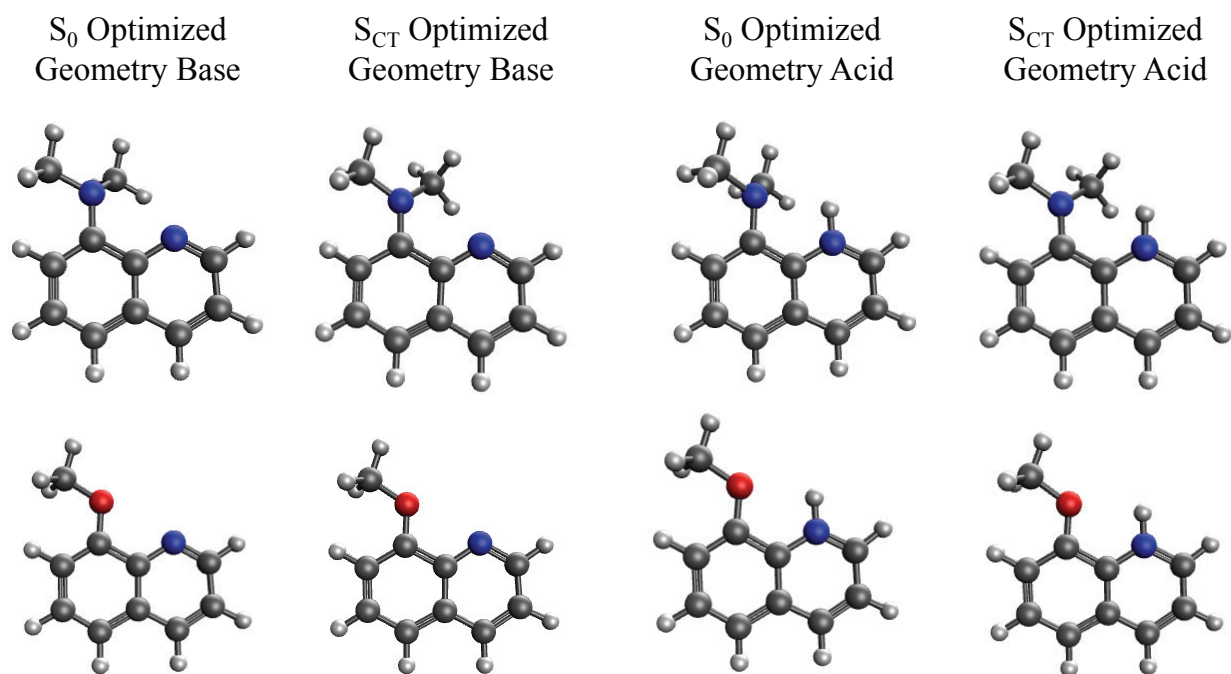
S$_0$ Optimized Geometry Base	S$_{CT}$ Optimized Geometry Base	S$_0$ Optimized Geometry Acid	S$_{CT}$ Optimized Geometry Acid

Figure S8: Optimized geometries on S$_0$ and S$_{CT}$ for the acidic and basic forms of 8-dimethylaminoquinoline and 8-methoxyquinoline. For 8-dimethylaminoquinoline, the major consequence of the excited state geometry optimization is the dimethylamine group becoming more planar. In the acidic forms, the –NC$_2$H$_6$ group is more affected by the neighboring N–H than the –OCH$_3$ group.
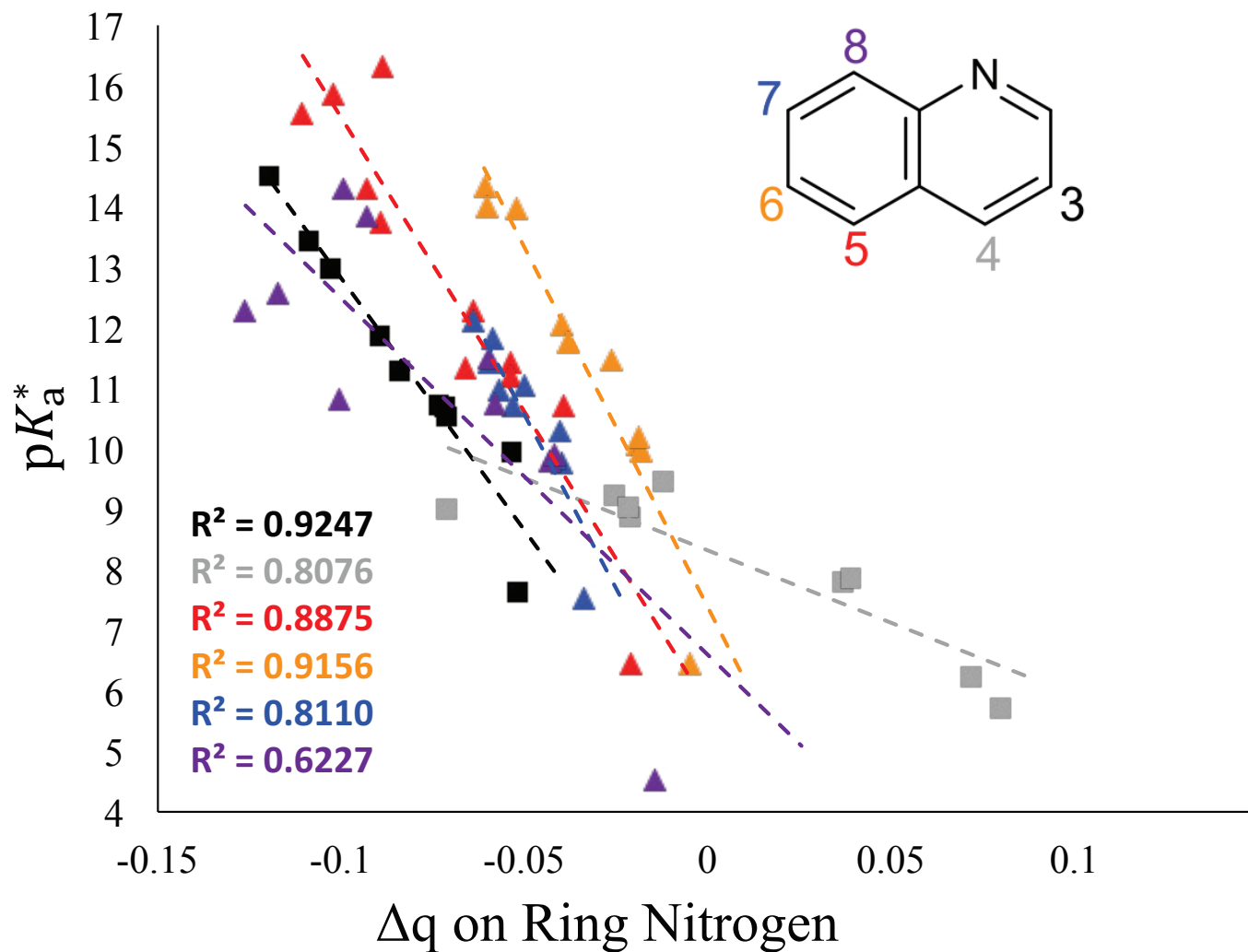
Figure S9: Plot of pK_a^* versus change in charge (Δq) on the ring nitrogen for all of the monosubstituted quinoline compounds considered in this study. Note that the pK_a^* are calculated using adiabatic energy gaps whereas the Δq on the ring nitrogen are calculated at the ground state geometry.

Table S7: Calculated ground state pK_a, excited state pK_a^*, vertical excitation energy, oscillator strength, and change in charge on the ring nitrogen at the ground-state (Δq) and excited-state (Δq^*) optimized geometries for the disubstituted quinoline compounds. The reported data is for the lowest energy $\pi \rightarrow \pi^*$ bright state and presented in order of increasing pK_a^*.

Substituents	Excitation Energy (eV)	Oscillator Strength	Δq on Ring N	Δq^* on Ring N	pK_a	pK_a^*
5-CH₃, 7-OCH₃	4.15	0.15	−0.067	−0.054	5.41	11.66
5-CH₃, 7-CH₃	4.47	0.10	−0.071	−0.052	5.18	12.36
5-CH₃, 6-CH₃	4.40	0.089	−0.051	−0.055	5.07	12.77
5-OCH₃, 7-OCH₃	4.02	0.14	−0.086	−0.068	5.44	12.91
5-CH₃, 6-OCH₃	4.07	0.11	−0.052	−0.066	4.95	13.42
4-NH₂, 5-NH₂	4.16	0.21	0.011	−0.084	7.88	13.58
6-NH₂, 7-NH₂	4.09	0.28	−0.060	−0.067	6.43	14.29
5-NH₂, 7-NH₂	3.71	0.11	−0.091	−0.078	6.80	14.44
5-CH₃, 6-NH₂	3.90	0.10	−0.060	−0.079	5.51	14.95
5-OCH₃, 7-CH₃	4.26	0.12	−0.096	−0.081	5.15	15.00
5-OCH₃, 6-CH₃	4.44	0.078	−0.050	−0.082	4.54	15.02
3-NH₂, 6-NH₂	4.04	0.20	−0.076	−0.087	5.30	15.28
5-NH₂, 7-OCH₃	3.93	0.10	−0.099	−0.088	5.97	15.29
4-CH₃, 5-NH₂	3.95	0.14	−0.086	−0.077	5.99	15.56
5-OCH₃, 6-OCH₃	4.09	0.10	−0.053	−0.088	4.55	15.78
5-OCH₃, 6-NH₂	3.87	0.10	−0.062	−0.084	5.12	15.94
5-NH₂, 7-CH₃	3.89	0.11	−0.104	−0.090	5.76	16.01
5-NHCH₃, 8-CH₃	3.63	0.14	−0.114	−0.108	5.35	16.08
5-NH₂, 8-CH₃	3.77	0.12	−0.108	−0.104	5.48	16.27
5-NHCH₃, 6-CH₃	3.78	0.12	−0.094	−0.089	5.46	16.28
5-NH₂, 6-CH₃	3.79	0.099	−0.102	−0.099	5.55	16.31
5-N(CH₃)₂, 8-CH₃	3.88	0.15	−0.094	−0.095	5.06	16.66
3-NH₂, 5-NH₂	3.72	0.12	−0.124	−0.123	5.23	16.72
5-NH₂, 6-OCH₃	3.62	0.097	−0.093	−0.101	5.41	16.79
3-N(CH₃)₂, 5-N(CH₃)₂	3.59	0.17	−0.120	−0.115	4.96	16.82
5-NHCH₃, 6-OCH₃	3.59	0.11	−0.089	−0.094	5.42	16.91
5-NH₂, 6-OH	3.69	0.098	−0.093	−0.103	5.39	16.93

Table S8: Calculated ground state pK_a, excited state pK_a^*, vertical excitation energy, oscillator strength, and change in charge on the ring nitrogen at the ground-state (Δq) and excited-state (Δq^*) optimized geometries for the disubstituted quinoline compounds, continued. The reported data is for the lowest energy $\pi \rightarrow \pi^*$ bright state and presented in order of increasing pK_a^*.

Substituents	Excitation Energy (eV)	Oscillator Strength	Δq on Ring N	Δq^* on Ring N	pK_a	pK_a^*
5-NHCH$_3$, 8-N(CH$_3$)$_2$	3.41	0.14	−0.121	−0.136	6.58	16.93
5-NH$_2$, 8-NC$_2$H$_6$	3.48	0.13	−0.118	−0.133	6.48	17.07
5-NHCH$_3$, 6-OH	3.66	0.11	−0.088	−0.097	5.38	17.09
3-NHCH$_3$, 5-NHCH$_3$	3.62	0.13	−0.138	−0.135	5.19	17.19
5-N(CH$_3$)$_2$, 8-N(CH$_3$)$_2$	3.55	0.16	−0.105	−0.125	5.89	17.53
5-NH$_2$, 8-OCH$_3$	3.61	0.10	−0.122	−0.125	5.54	17.70
5-NHCH$_3$, 8-OCH$_3$	3.51	0.11	−0.126	−0.128	5.65	18.00
5-N(CH$_3$)$_2$, 8-OCH$_3$	3.77	0.12	−0.110	−0.116	5.18	18.01
5-NHCH$_3$, 6-NHCH$_3$	3.62	0.11	−0.069	−0.096	5.51	18.10
5-NH$_2$, 6-NH$_2$	3.59	0.079	−0.092	−0.111	5.57	18.16
5-NHCH$_3$, 6-NH$_2$	3.78	0.094	−0.0700	−0.100	5.36	18.22

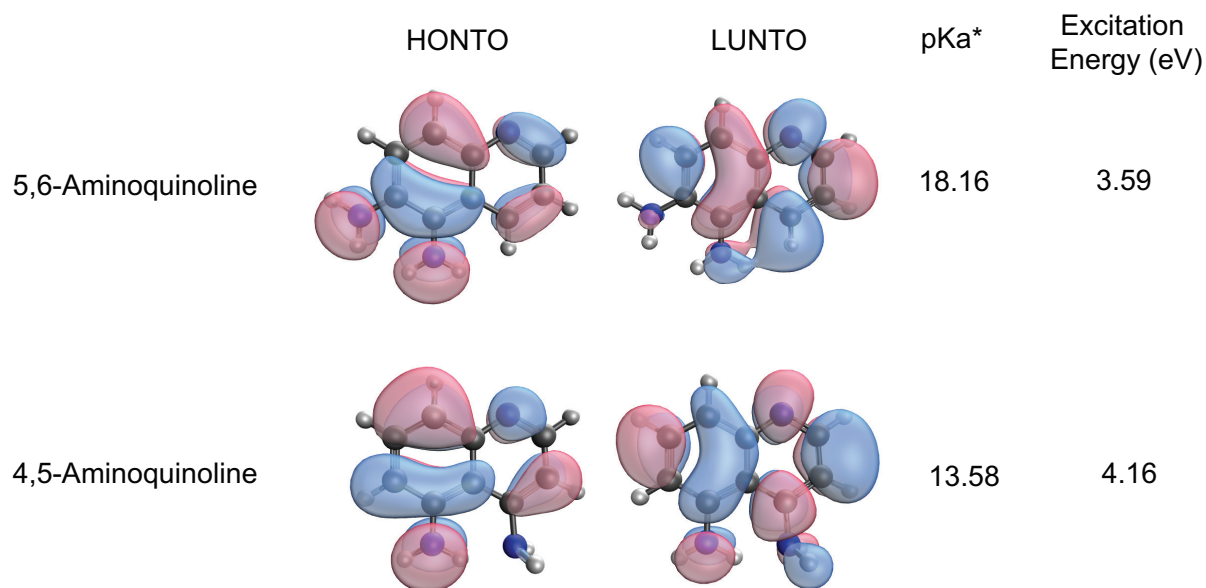|	HONTO	LUNTO	pKa*	Excitation Energy (eV)
5,6-Aminoquinoline			18.16	3.59
4,5-Aminoquinoline			13.58	4.16

Figure S10: The highest occupied natural transition orbital (HONTO) and lowest unoccupied natural transition orbital (LUNTO) at the excited state optimized geometry, along with the pK_a^* and vertical excitation energy, for 5,6-aminoquinoline and 4,5-aminoquinoline.
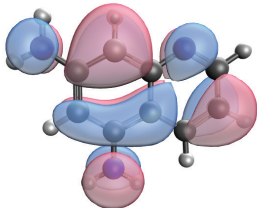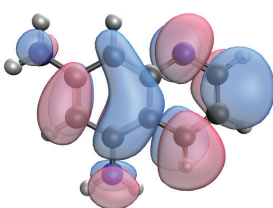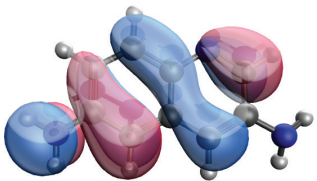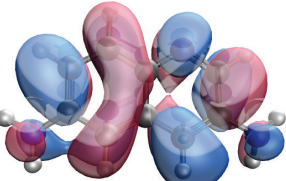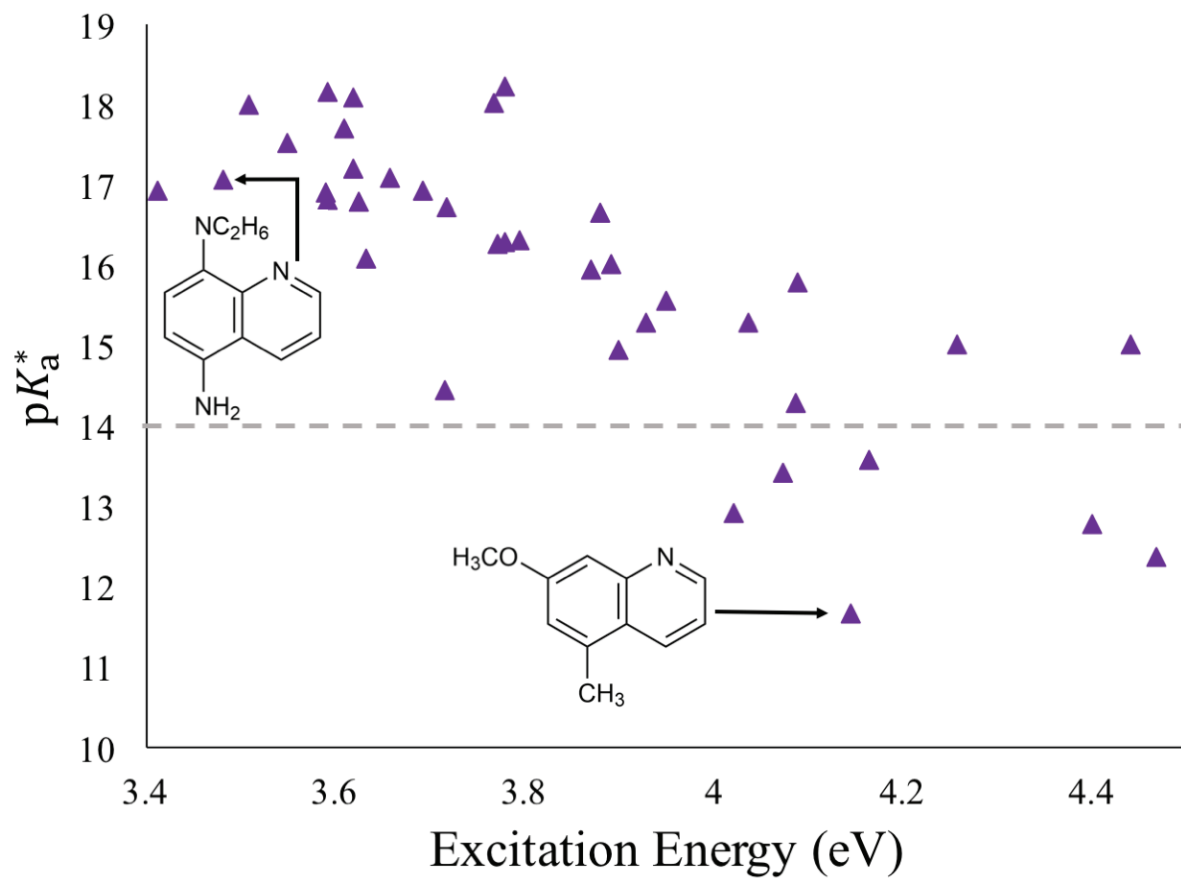
	HONTO	LUNTO	pKa*	Excitation Energy (eV)
5,7-Aminoquinoline			14.44	3.72
3,6-Aminoquinoline			15.28	4.04

Figure S11: The highest occupied natural transition orbital (HONTO) and lowest unoccupied natural transition orbital (LUNTO) at the excited state optimized geometry, along with the pK_a^* and vertical excitation energy, for 5,7-aminoquinoline and 3,6-aminoquinoline.

Figure S12: Plot of pK_a^* versus vertical excitation energy for the disubstituted quinoline compounds. Recall that all compounds with $pK_a^* > 14$ are strong bases in the excited state.
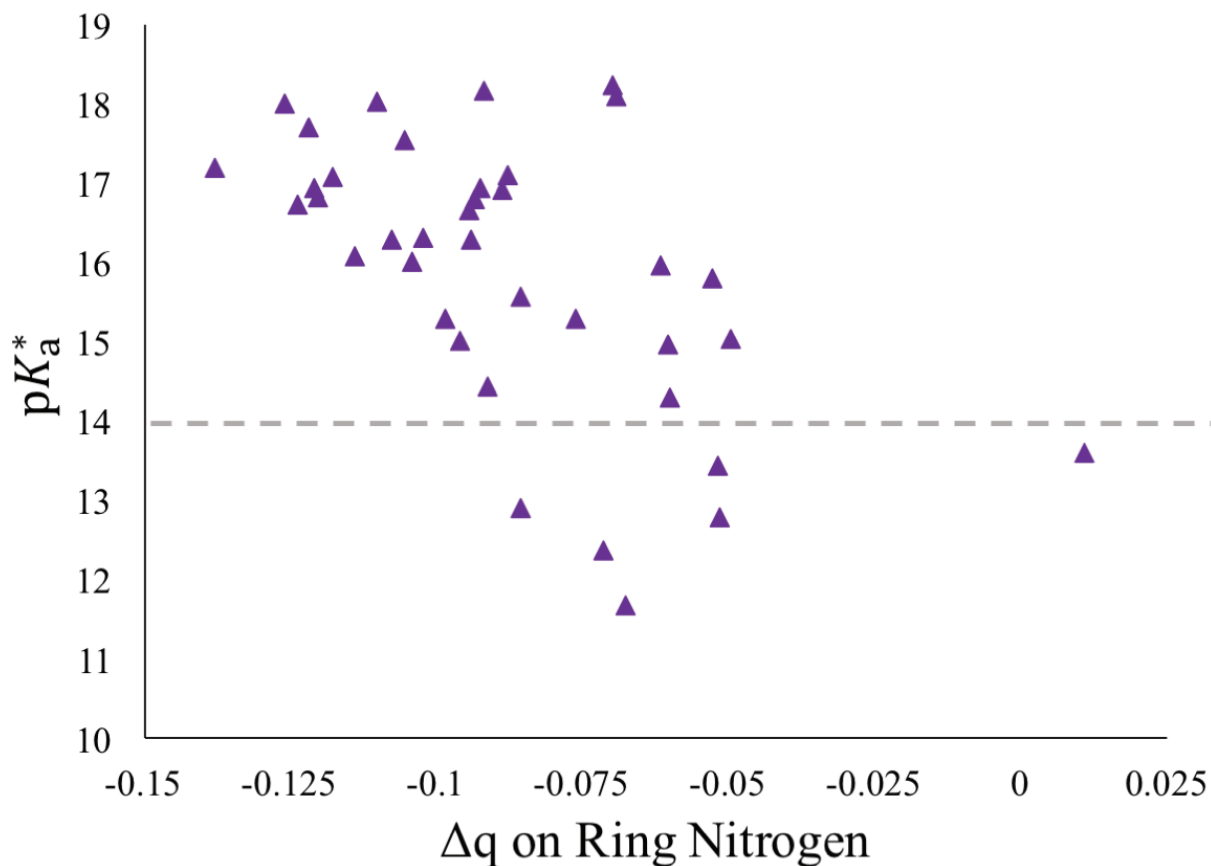
Figure S13: Plot of pK_a^* versus change in charge (Δq) on the ring nitrogen for the disubstituted quinoline compounds. Note that the pK_a^* are calculated using adiabatic energy gaps whereas the Δq on the ring N are calculated at the ground state geometry. While there is some correlation between pK_a^* and Δq on the ring N, the trend is too noisy to allow a calculated Δq on the ring N to accurately predict pK_a^*.
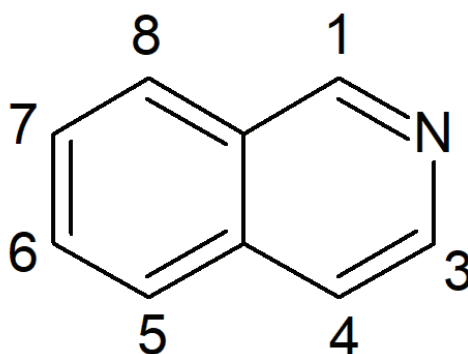

Figure S14: Substituent position numbering system for the isoquinoline compounds.

Table S9: Calculated ground state pK_a, excited state pK_a^*, vertical excitation energy, oscillator strength, and change in charge (Δq) on the ring nitrogen for the isoquinoline compounds. The reported data is for the lowest energy $\pi \rightarrow \pi^*$ bright state. The monosubstituted and disubstituted compounds are each reported in order of increasing pK_a^*.

Substituent	Excitation Energy (eV)	Oscillator Strength	Δq on Ring N	pK_a	pK_a^*
4-NH2	4.07	0.18	−0.065	5.49	8.06
4-OCH3	4.43	0.12	−0.084	4.44	8.72
4-CH3	4.44	0.12	−0.083	5.03	9.23
6-OCH$_3$	4.43	0.081	0.002	5.46	9.87
6-CH$_3$	4.55	0.066	−0.085	5.13	10.18
6-NH$_2$	4.18	0.079	0.012	6.32	10.30
6-NHCH$_3$	4.11	0.076	0.013	6.35	10.40
7-CH$_3$	4.41	0.076	−0.089	4.99	10.81
5-CH$_3$	4.43	0.11	−0.093	4.83	10.95
7-OCH$_3$	4.08	0.094	−0.092	4.95	11.48
8-CH$_3$	4.40	0.12	−0.093	5.02	11.70
7-NHCH$_3$	3.63	0.091	−0.093	5.39	13.12
5-OCH$_3$	4.25	0.12	−0.110	4.71	13.38
7-NH$_2$	3.87	0.080	−0.093	5.55	13.43
8-OCH$_3$	4.25	0.16	−0.102	5.06	13.75
5-NH$_2$	3.95	0.14	−0.110	4.90	14.86
8-NHCH$_3$	3.76	0.19	−0.110	5.40	14.90
5-NHCH$_3$	3.81	0.14	−0.114	4.72	14.93
8-NH$_2$	3.90	0.15	−0.108	5.52	15.12
6-NH$_2$, 7-NH$_2$	4.15	0.099	−0.065	6.61	13.29
5-NH$_2$, 6-NH$_2$	3.83	0.092	−0.053	5.96	14.88
5-NH$_2$, 7-NH$_2$	3.67	0.093	−0.114	5.61	15.49
7-NH$_2$, 8-NH$_2$	3.54	0.11	−0.115	5.83	16.61
5-NH$_2$, 8-NH$_2$	3.46	0.14	−0.118	5.32	16.82
5-NHCH$_3$, 8-NHCH$_3$	3.35	0.15	−0.122	5.40	17.48
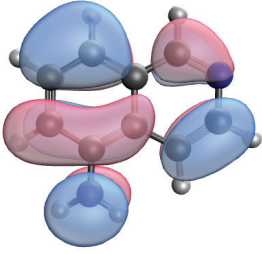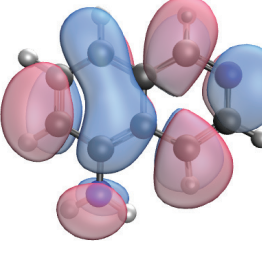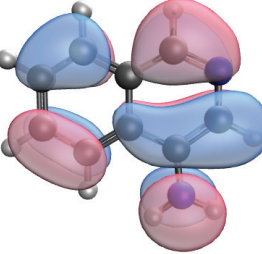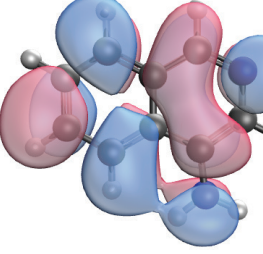
	HONTO	LUNTO	pKa*	Excitation Energy (eV)
5-Amino-isoquinoline			14.86	3.95
4-Amino-isoquinoline			8.06	4.07

Figure S15: The highest occupied natural transition orbital (HONTO) and lowest unoccupied natural transition orbital (LUNTO) at the excited state optimized geometry, along with the pK_a^* and vertical excitation energy, for 5-amino-isoquinoline and 4-amino-isoquinoline.
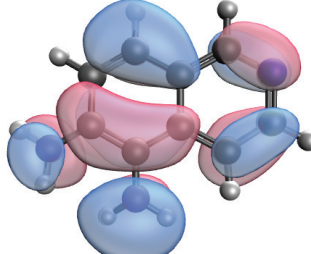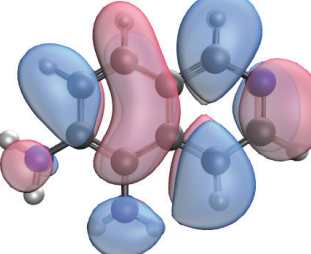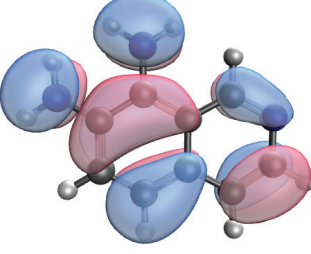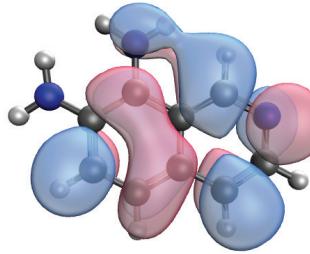

	HONTO	LUNTO	pKa*	Excitation Energy (eV)
5,6-Amino-isoquinoline			14.88	3.83
7,8-Amino-isoquinoline			16.61	3.54

Figure S16: The highest occupied natural transition orbital (HONTO) and lowest unoccupied natural transition orbital (LUNTO) at the excited state optimized geometry, along with the pK_a^* and vertical excitation energy, for 5,6-amino-isoquinoline and 7,8-amino-isoquinoline.
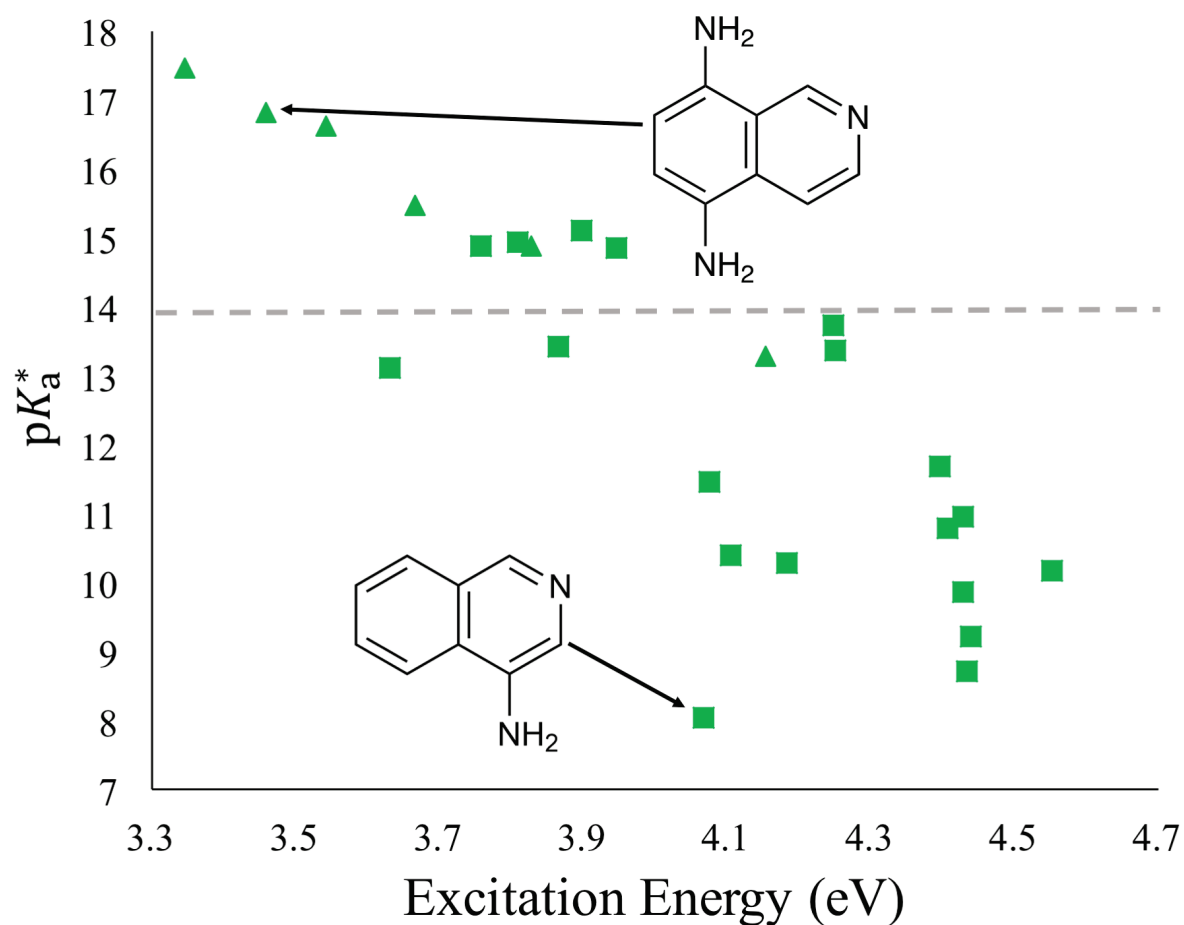
Figure S17: Plot of pK_a^* versus vertical excitation energy for the isoquinoline compounds. The square data points represent monosubstituted isoquinoline compounds whereas the triangles are disubstituted isoquinoline compounds. Recall that all compounds with $pK_a^* > 14$ are strong bases in the excited state.
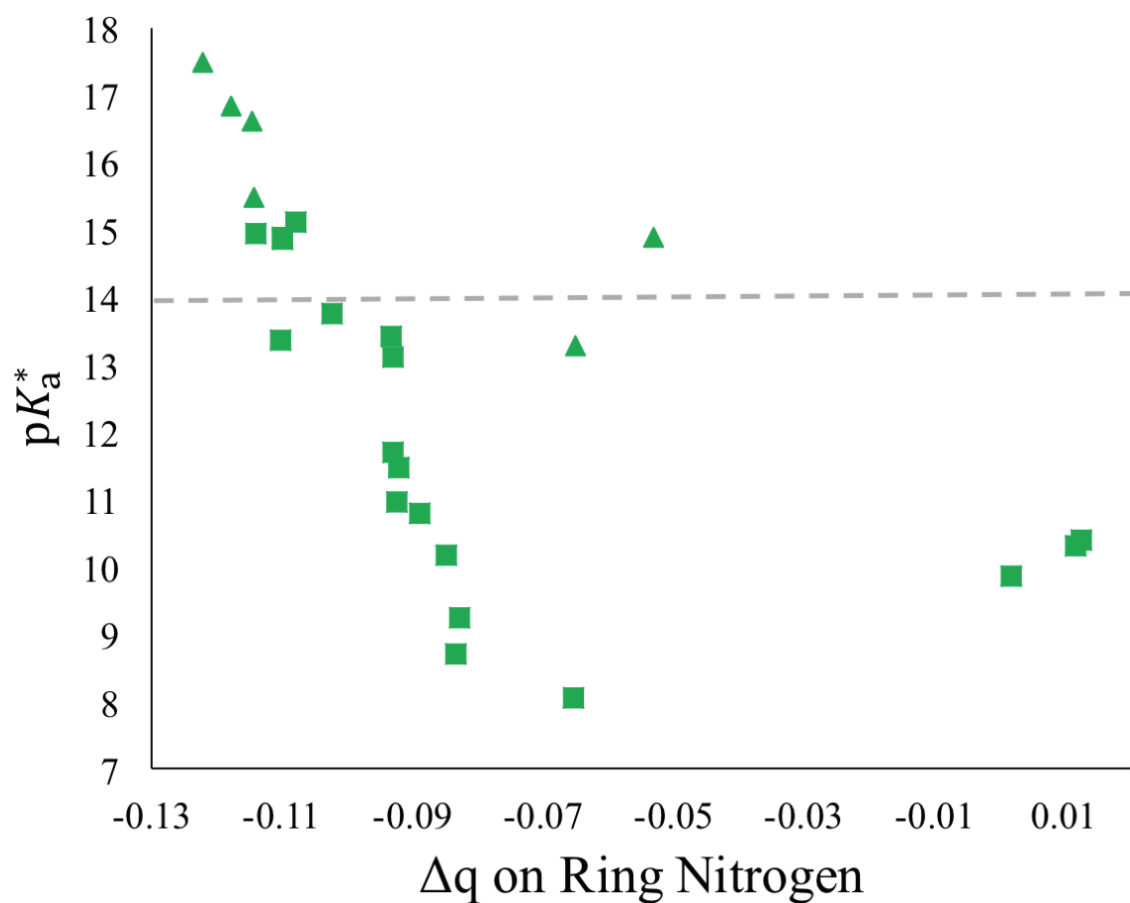
Figure S18: Plot of pK_a^* versus change in charge (Δq) on the ring nitrogen for the isoquinoline compounds. The square data points represent monosubstituted isoquinoline compounds whereas the triangles are disubstituted isoquinoline compounds. Note that the pK_a^* are calculated using adiabatic energy gaps whereas the Δq on the ring N are calculated at the ground state geometry. While there is some correlation between pK_a^* and Δq on the ring N, the trend is too noisy to allow a calculated Δq on the ring N to accurately predict pK_a^*.
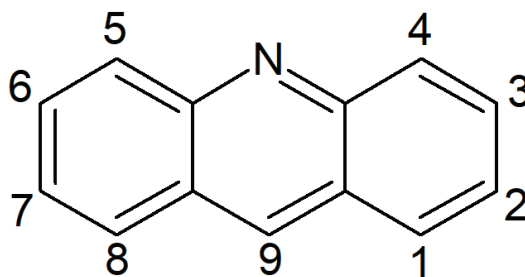
Figure S19: Substituent position numbering system for the acridine compounds.

Table S10: Calculated ground state pK_a, excited state pK_a^*, vertical excitation energy, oscillator strength, and change in charge on the ring nitrogen at the ground-state (Δq) and excited-state (Δq^*) optimized geometries for the acridine compounds. The reported data is for the lowest energy $\pi \rightarrow \pi^*$ bright state. The monosubstituted and disubstituted compounds are each reported in order of increasing pK_a^*.

Substituents	Excitation Energy (eV)	Oscillator Strength	Δq on Ring N	Δq^* on Ring N	pK_a	pK_a^*
1-H	3.64	0.093	0.001	0.018	5.40	7.84
1-NHCH$_3$	3.15	0.13	−0.048	−0.024	6.24	12.30
1-NH$_2$	3.17	0.12	−0.051	−0.036	6.19	12.32
1-NH$_2$,3-NH$_2$	3.08	0.15	−0.015	0.004	7.95	10.38
3-NH$_2$, 6-NH$_2$	3.59	0.49	−0.049	0.051	8.48	11.04
1-NH$_2$, 8-NH$_2$	3.07	0.13	−0.046	−0.022	6.90	12.11
1-NH$_2$, 2-OCH$_3$	2.92	0.090	−0.066	−0.059	5.90	13.66
1-NH$_2$, 4-NC$_2$H$_6$	2.87	0.11	−0.084	−0.097	7.09	13.72
2-NHCH$_3$, 7-NHCH$_3$	3.04	0.050	−0.079	−0.073	5.91	13.76
1-NH$_2$, 2-OH	3.00	0.090	−0.068	−0.061	5.87	14.06
2-NH$_2$, 7-NH$_2$	3.29	0.053	−0.071	−0.071	6.02	14.07
2-N(CH$_3$)$_2$, 7-N(CH$_3$)$_2$	3.10	0.034	−0.083	−0.075	5.98	14.18
1-N(CH$_3$)$_2$, 4-N(CH$_3$)$_2$	2.97	0.13	−0.082	−0.092	6.46	14.52
1-NH$_2$, 4-OCH$_3$	2.96	0.094	−0.083	−0.078	6.15	14.65
1-NH$_2$, 2-NH$_2$	2.91	0.077	−0.074	−0.085	6.27	15.11
1-N(CH$_3$)$_2$, 2-N(CH$_3$)$_2$	2.97	0.088	−0.067	−0.078	5.83	15.80
1-NHCH$_3$, 2-NHCH$_3$	2.97	0.11	−0.067	−0.074	5.56	16.21
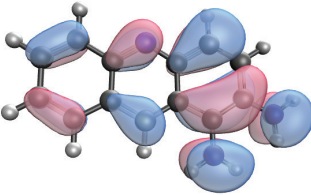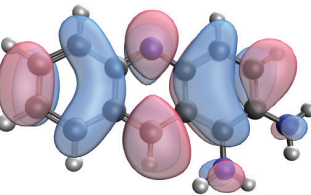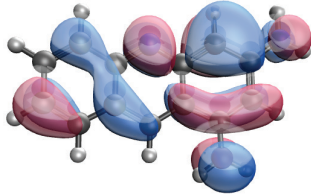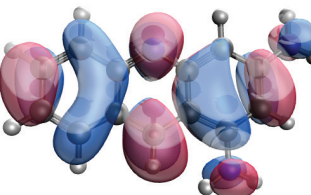
	HONTO	LUNTO	pKa*	Excitation Energy (eV)
1,2-Amino-acridine			15.11	2.91
1,3-Amino-acridine			10.38	3.08

Figure S20: The highest occupied natural transition orbital (HONTO) and lowest unoccupied natural transition orbital (LUNTO) at the excited state optimized geometry, along with the pK_a^* and vertical excitation energy, for 1,2-amino-acridine and 1,3-amino-acridine.
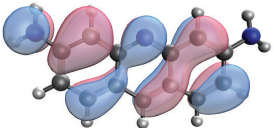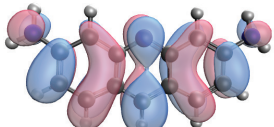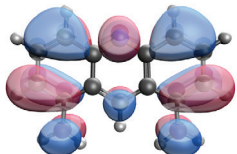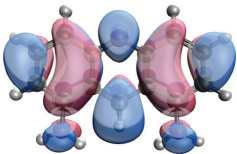
	HONTO	LUNTO	pKa*	Excitation Energy (eV)
3,6-Amino-acridine			11.04	3.59
2,7-Amino-acridine			14.07	3.30
1,8-Amino-acridine			12.11	3.07

Figure S21: The highest occupied natural transition orbital (HONTO) and lowest unoccupied natural transition orbital (LUNTO) at the excited state optimized geometry, along with the pK_a^* and vertical excitation energy, for 3,6-amino-acridine, 2,7-amino-acridine, and 1,8-amino-acridine.
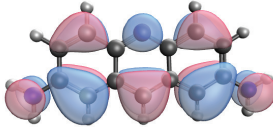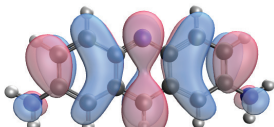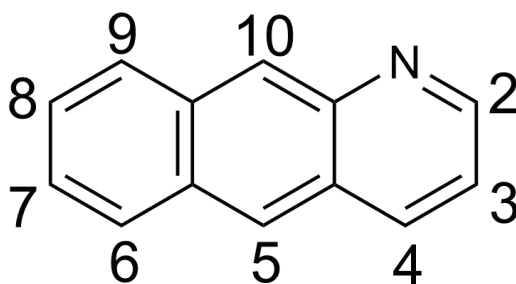
Figure S22: Substituent position numbering system for the 1-azaanthracene compounds.

Table S11: Calculated ground state pK_a, excited state pK_a^*, vertical excitation energy, oscillator strength, and change in charge on the ring nitrogen (Δq) for the monosubstituted 1-azaanthracene compounds. The reported data is for the lowest energy $\pi \rightarrow \pi^*$ bright state and the compounds are reported in order of increasing pK_a^*.

Substituents	Excitation Energy (eV)	Oscillator Strength	Δq on Ring N	pK_a	pK_a^*
5-H	3.55	0.093	−0.022	4.73	10.04
5-NH_2	2.97	0.12	−0.052	5.47	11.51
8-$NHCH_3$	3.23	0.14	−0.037	5.49	11.80
5-$NHCH_3$	3.01	0.14	−0.045	5.99	11.84
8-$N(CH_3)_2$	3.12	0.16	−0.036	5.54	11.91
5-$N(CH_3)_2$	2.99	0.14	−0.041	5.03	11.95
8-NH_2	3.28	0.13	−0.034	5.69	12.15
7-$NHCH_3$	3.19	0.11	−0.030	5.04	12.37
7-$N(CH_3)_2$	3.09	0.13	−0.029	5.13	12.52
9-$NHCH_3$	3.10	0.12	−0.038	4.53	12.53
7-NH_2	3.26	0.10	−0.027	5.15	12.57
9-NH_2	3.21	0.11	−0.034	4.72	12.64
9-$N(CH_3)_2$	3.33	0.13	−0.029	4.77	12.91
6-NH_2	3.20	0.12	−0.034	4.97	13.55
6-$N(CH_3)_2$	3.33	0.14	−0.031	4.81	13.89
6-$NHCH_3$	3.36	0.12	−0.030	4.72	14.25

Table S12: Calculated ground state pK_a, excited state pK_a^*, vertical excitation energy, oscillator strength, and change in charge on the ring nitrogen at the ground-state (Δq) and excited-state (Δq^*) optimized geometries for the disubstituted 1-azaanthracene compounds, continued. The reported data is for the lowest energy $\pi \rightarrow \pi^*$ bright state and the compounds are reported in order of increasing pK_a^*.

Substituents	Excitation Energy (eV)	Oscillator Strength	Δq on Ring N	Δq^* on Ring N	pK_a	pK_a^*
7-OCH$_3$, 8-OCH$_3$	3.55	0.078	−0.032	−0.018	4.97	10.76
5-OCH$_3$, 6-OCH$_3$	3.31	0.13	−0.039	−0.027	4.77	12.14
7-N(CH$_3$)$_2$, 8-N(CH$_3$)$_2$	3.32	0.033	−0.035	−0.031	5.31	12.28
5-NH$_2$, 6-NH$_2$	2.91	0.13	−0.059	−0.041	6.04	12.87
6-OCH$_3$, 7-OCH$_3$	3.29	0.098	−0.024	−0.022	4.71	12.87
7-NHCH$_3$, 8-NHCH$_3$	3.28	0.092	−0.032	−0.033	5.46	12.89
7-NH$_2$, 8-NH$_2$	3.35	0.050	−0.038	−0.031	5.74	12.95
5-NHCH$_3$, 6-NHCH$_3$	2.96	0.15	−0.049	−0.031	6.74	13.00
6-OCH$_3$, 9-OCH$_3$	3.25	0.10	−0.036	−0.031	4.67	13.25
5-N(CH$_3$)$_2$, 6-N(CH$_3$)$_2$	2.91	0.17	−0.045	−0.033	5.41	13.37
6-N(CH$_3$)$_2$, 7-N(CH$_3$)$_2$	3.05	0.092	−0.032	−0.034	4.77	14.25
6-NH$_2$, 7-NH$_2$	2.98	0.078	−0.035	−0.037	5.21	14.47
6-NH$_2$, 9-NH$_2$	2.87	0.10	−0.038	−0.038	4.80	14.60
6-NHCH$_3$, 7-NHCH$_3$	2.98	0.11	−0.030	−0.037	5.12	15.01
6-NHCH$_3$, 9-NHCH$_3$	2.79	0.11	−0.040	−0.040	4.94	15.05
6-N(CH$_3$)$_2$, 9-N(CH$_3$)$_2$	3.11	0.15	−0.034	−0.040	4.70	15.17
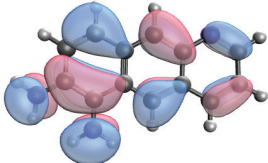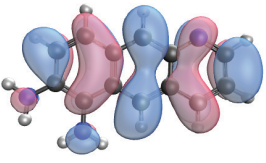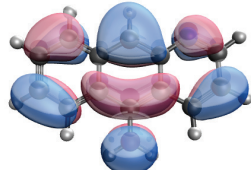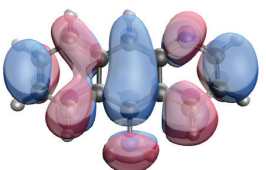
	HONTO	LUNTO	pKa*	Excitation Energy (eV)
6,7-Amino-1-azaanthracene			14.47	2.98
5-Amino-1-azaanthracene			11.51	2.97

Figure S23: The highest occupied natural transition orbital (HONTO) and lowest unoccupied natural transition orbitas (LUNTO) at the excited state optimized geometry, along with the pK_a^* and vertical excitation energy, for 6,7-amino-1-azaanthracene and 5-amino-1-azaanthracene.
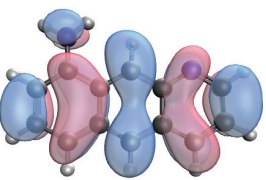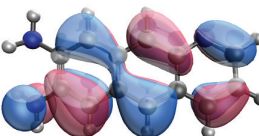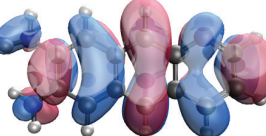
	HONTO	LUNTO	pKa*	Excitation Energy (eV)
9-Amino-1-azaanthracene			13.96	3.94
7,8-Amino-1-azaanthracene			11.81	3.99

Figure S24: The highest occupied natural transition orbital (HONTO) and lowest unoccupied natural transition orbitals (LUNTO) at the excited state optimized geometry, along with the pK_a^* and vertical excitation energy, for 7,8-amino-1-azaanthracene and 9-amino-1-azaanthracene.
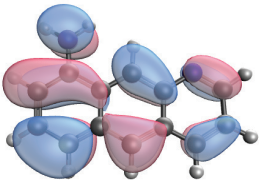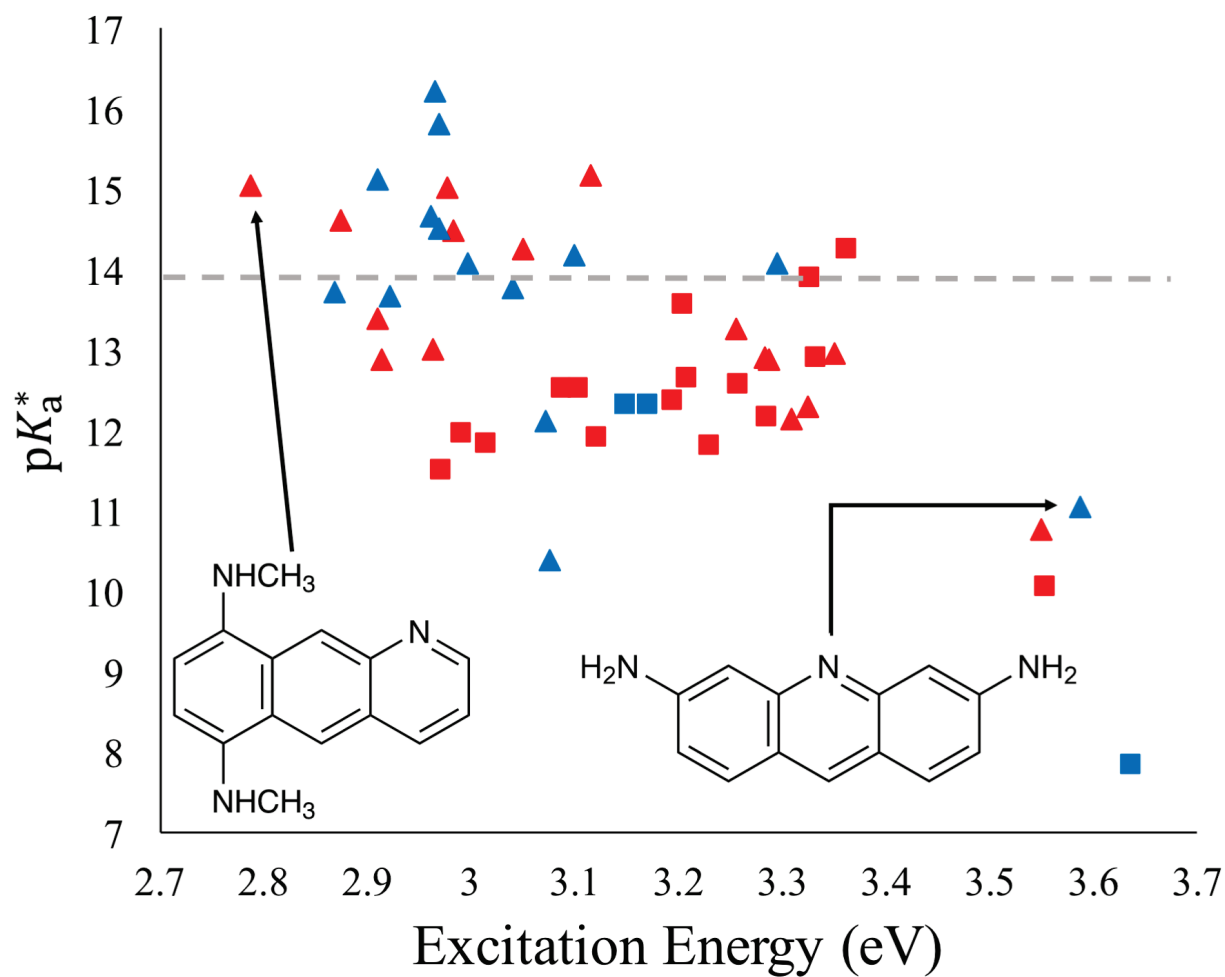
Figure S25: Plot of pK_a^* versus vertical excitation energy for the acridine (blue data points) and 1-azaanthracene (red data points) compounds. The monosubstituted compounds are represented by squares while the disubstituted compounds are shown as triangles. Recall that all compounds with $pK_a^* > 14$ are strong bases in the excited state.
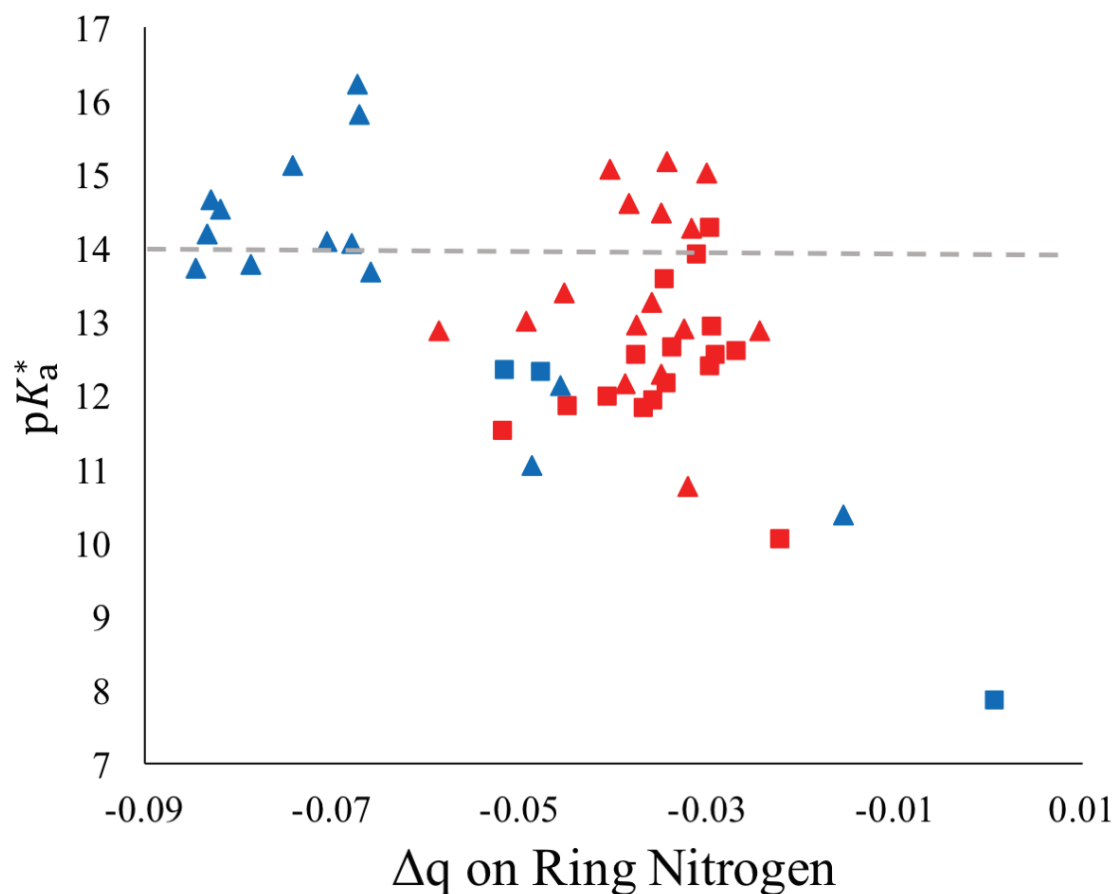
Figure S26: Plot of pK_a^* versus change in charge (Δq) on the ring nitrogen for the acridine (blue data points) and 1-azaanthracene (red data points) compounds. The monosubstituted compounds are represented by squares while the disubstituted compounds are shown as triangles. Note that the pK_a^* are calculated using adiabatic energy gaps whereas the Δq on the ring N are calculated at the ground state geometry. While there is some correlation between pK_a^* and Δq on the ring N, the trend is too noisy to allow a calculated Δq on the ring N to accurately predict pK_a^*.
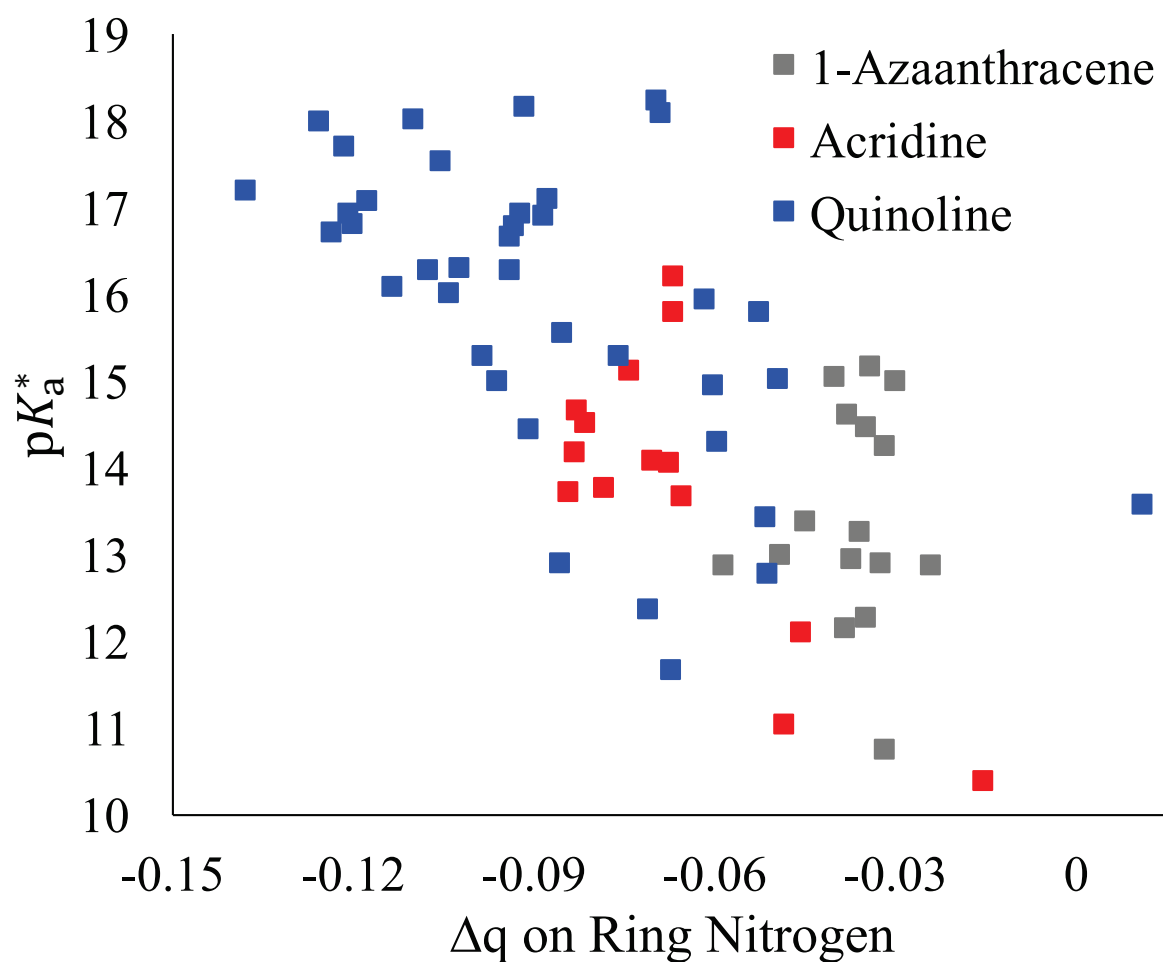
Figure S27: Plot of pK_a^* versus change in charge (Δq) on the ring nitrogen for the disubstituted 1-azaanthracene (gray squares), acridine (red squares), and quinoline (blue squares) compounds. Note that the pK_a^* are calculated using adiabatic energy gaps whereas the Δq on the ring N are calculated at the ground state geometry. Linear regression analysis leads to R^2 values of 0.004, 0.56, and 0.33 for the 1-azaanthracene, acridine, and quinoline compounds respectively.

Table S13: Calculated E_{SCT} and $E_T - E_{SCT}$ between S_{CT} and the two closest triplet states for representative 5-R and 6-R quinoline compounds at the S_{CT} optimized geometries. Because the Tamm-Dancoff approximation (TDA) is known to minimize triplet instability problems that can appear in TDDFT calculations, all of these energies were calculated using TDA.[2] The E_{SCT} is reported relative to the ground state.

Compound	E_{SCT} (eV)	Closest Triplet $E_T - E_{SCT}$ (eV)	Second Closest Triplet $E_T - E_{SCT}$ (eV)
5-methoxyquinoline	3.75	0.16	0.26
5-methoxyquinoline acid	3.18	0.47	0.72
5-aminoquinoline	3.30	0.21	0.69
5-aminoquinoline acid	2.72	0.69	–0.78
5-methylaminoquinoline	3.29	0.24	0.69
5-methylaminoquinoline acid	2.69	0.72	–0.75
5-dimethylaminoquinoline	3.30	0.27	0.57
5-dimethylaminoquinoline acid	2.69	0.73	–0.79
6-aminoquinoline	3.57	–0.08	0.26
6-aminoquinoline acid	3.05	0.21	0.74
6-methylaminoquinoline	3.58	–0.16	0.23
6-methylaminoquinoline acid	3.04	0.19	0.72
6-dimethylaminoquinoline	3.49	–0.05	0.32
6-methylaminoquinoline acid	2.92	0.28	0.81

Table S14: Calculated E_{SCT} and $E_T - E_{SCT}$ between S_{CT} and the two closest triplet states for representative disubstituted quinoline compounds at the S_{CT} optimized geometries. Because the Tamm-Dancoff approximation (TDA) is known to minimize triplet instability problems that can appear in TDDFT calculations, all of these energies were calculated using TDA.[2] The E_{SCT} is reported relative to the ground state.

Compound	E_{SCT} (eV)	Closest Triplet $E_T - E_{SCT}$ (eV)	Second Closest Triplet $E_T - E_{SCT}$ (eV)
3-NH$_2$, 5-NH$_2$	3.23	−0.0004	0.22
3-NH$_2$, 5-NH$_2$ acid	2.61	0.21	0.82
3-NH$_2$, 6-NH$_2$	3.67	0.33	0.46
3-NH$_2$, 6-NH$_2$ acid	3.06	0.67	−0.73
4-NH$_2$, 5-NH$_2$	3.27	0.12	0.67
4-NH$_2$, 5-NH$_2$ acid	2.93	0.43	0.66
3-NC$_2$H$_6$, 5-NC$_2$H$_6$	3.21	−0.09	0.26
3-NC$_2$H$_6$, 5-NC$_2$H$_6$ acid	2.57	0.09	0.83
5-NC$_2$H$_6$, 8-NC$_2$H$_6$	2.56	0.28	−0.87
5-NC$_2$H$_6$, 8-NC$_2$H$_6$ acid	1.81	−0.63	0.85
5-NC$_2$H$_6$, 8-OCH$_3$	2.88	0.21	−0.95
5-NC$_2$H$_6$, 8-OCH$_3$ acid	2.19	−0.69	0.73
5-NH$_2$, 8-OCH$_3$	2.80	0.19	−0.93
5-NH$_2$, 8-OCH$_3$ acid	2.13	−0.68	0.74
5-OCH$_3$, 6-NH$_2$	3.38	0.10	0.32
5-OCH$_3$, 6-NH$_2$ acid	2.50	0.70	0.88
6-NH$_2$, 7-NH$_2$	3.73	0.21	0.49
6-NH$_2$, 7-NH$_2$ acid	3.25	−0.41	0.59
5-NH$_2$, 6-NH$_2$	2.87	0.40	0.70
5-NH$_2$, 6-NH$_2$ acid	2.13	−0.74	0.92
5-NH$_2$, 7-NH$_2$	3.21	0.32	0.43
5-NH$_2$, 7-NH$_2$ acid	2.80	0.29	−0.72
5-NH$_2$, 6-OCH$_3$	3.05	0.42	0.73
5-NH$_2$, 6-OCH$_3$ acid	2.37	−0.77	0.88
5-NH$_2$, 7-OCH$_3$	3.37	0.30	0.43
5-NH$_2$, 7-OCH$_3$ acid	2.85	0.53	−0.71

Table S15: Calculated E_{SCT} and $E_T - E_{SCT}$ between S_{CT} and the two closest triplet states for representative disubstituted acridine compounds at the S_{CT} optimized geometries. Because the Tamm-Dancoff approximation (TDA) is known to minimize triplet instability problems that can appear in TDDFT calculations, all of these energies were calculated using TDA.[2] The E_{SCT} is reported relative to the ground state.

Compound	E_{SCT} (eV)	Closest Triplet $E_T - E_{SCT}$ (eV)	Second Closest Triplet $E_T - E_{SCT}$ (eV)
2-NC$_2$H$_6$, 7-NC$_2$H$_6$	2.92	0.48	–0.56
2-NC$_2$H$_6$, 7-NC$_2$H$_6$ acid	2.45	–0.52	0.76
1-NH$_2$, 2-NH$_2$	2.31	0.57	0.94
1-NH$_2$, 2-NH$_2$ acid	1.76	–0.78	1.08
1-NH$_2$, 2-OH	2.52	0.40	0.85
1-NH$_2$, 2-OH acid	2.07	0.75	–0.81
1-NC$_2$H$_6$, 2-NC$_2$H$_6$	2.35	0.42	0.76
1-NC$_2$H$_6$, 2-NC$_2$H$_6$ acid	1.75	–0.74	0.88
1-NH$_2$, 4-NC$_2$H$_6$	1.94	0.80	–0.84
1-NH$_2$, 4-NC$_2$H$_6$ acid	1.52	–0.69	1.22
1-NH$_2$, 4-OCH$_3$	2.28	0.58	0.76
1-NH$_2$, 4-OCH$_3$ acid	1.88	–0.74	0.89
1-NHCH$_3$, 2-NHCH$_3$	2.30	0.55	0.94
1-NHCH$_3$, 2-NHCH$_3$ acid	1.70	–0.81	1.12

Table S16: Calculated E_{SCT} and $E_T - E_{SCT}$ between S_{CT} and the two closest triplet states for representative 1-azaanthracene compounds at the S_{CT} optimized geometries. Because the Tamm-Dancoff approximation (TDA) is known to minimize triplet instability problems that can appear in TDDFT calculations, all of these energies were calculated using TDA.[2] The E_{SCT} is reported relative to the ground state.

Compound	E_{SCT} (eV)	Closest Triplet $E_T - E_{SCT}$ (eV)	Second Closest Triplet $E_T - E_{SCT}$ (eV)
$6NHCH_3, 9NHCH_3$	2.03	0.67	0.75
$6NHCH_3, 9NHCH_3$ acid	1.43	−0.63	1.00
$6NH_2, 9NH_2$	2.01	0.62	0.80
$6NH_2, 9NH_2$ acid	1.44	−0.70	0.96
$6NC_2H_6, 9NC_2H_6$	2.12	0.61	0.66
$6NC_2H_6, 9NC_2H_6$ acid	1.46	−0.65	0.99
$6NHCH_3, 7NHCH_3$	2.22	0.53	0.86
$6NHCH_3, 7NHCH_3$ acid	1.60	−0.72	0.97
$6NH_2, 7NH_2$	2.47	0.29	0.75
$6NH_2, 7NH_2$ acid	1.83	0.73	−0.73
$6NC_2H_6, 7NC_2H_6$	2.39	0.48	0.77
$6NC_2H_6, 7NC_2H_6$ acid	1.79	−0.76	0.90
$6NHCH_3$	2.64	0.33	0.58
$6NHCH_3$ acid	2.15	0.68	−0.84

Table S16: Calculated excited state energy (E_{SCT}), radical anion energy ($E_{radical\ anion}$), and exited state electron affinity ($E_{radical\ anion} - E_{SCT}$) for a range of nitrogen-containing heterocyclic compounds. All electronic energies are evaluated at the excited state optimized geometry. The excited state electron affinity should be compared with the ionization potential of liquid water, 6.5 ± 0.5 eV.[3]

Compound	E_{SCT} (kcal mol^{-1})	$E_{radical\ anion}$ (kcal mol^{-1})	$E_{radical\ anion} - E_{SCT}$ (eV)
5-cyanoquinoline	–310009.90	–310163.47	–6.66
5-chloroquinoline	–540534.95	–540678.26	–6.21
quinoline	–252121.26	–252264.35	–6.21
5-methylquinoline	–276799.38	–276937.60	–5.99
5-methoxyquinoline	–324004.80	–324134.63	–5.63
5-aminoquinoline	–286887.59	–287005.40	–5.11
5-dimethylaminoquinoline	–336213.02	–336330.42	–5.09
5,6-aminoquinoline	–321637.97	–321742.47	–4.53
1,2-amino-acridine	–418061.09	–418165.45	–4.53
6,7-amino-1-azaanthracene	–418058.06	–418162.18	–4.51

(1)   Driscoll, E. W.; Hunt, J. R.; Dawlaty, J. M. Photobasicity in Quinolines: Origin and Tunability via the Substituents' Hammett Parameters. *J. Phys. Chem. Lett.* **2016**, *7* (11), 2093–2099. https://doi.org/10.1021/acs.jpclett.6b00790.

(2)   Peach, M. J. G.; Williamson, M. J.; Tozer, D. J. Influence of Triplet Instabilities in TDDFT. *J. Chem. Theory Comput.* **2011**, *7* (11), 3578–3585. https://doi.org/10.1021/ct200651r.

(3)   Roy, S.; Ardo, S.; Furche, F. 5-Methoxyquinoline Photobasicity Is Mediated by Water Oxidation. *J. Phys. Chem. A* **2019**, *123* (31), 6645–6651. https://doi.org/10.1021/acs.jpca.9b05341.